


# New constraints on the last deglaciation of the Cordilleran Ice Sheet in coastal Southeast Alaska

Alia J. Lesnek<sup>a\*</sup> , Jason P. Briner<sup>a</sup>, James F. Baichtal<sup>b</sup>, Alex S. Lyles<sup>b</sup>

<sup>a</sup>Department of Geology, University at Buffalo, Buffalo, NY, 14209, USA

<sup>b</sup>Tongass National Forest, Thorne Bay, AK 99919, USA

\*Corresponding author at: University of New Hampshire, Department of Earth Sciences, Durham, NH 03824, USA. E-mail: [alia.lesnek@unh.edu](mailto:alia.lesnek@unh.edu) (Alia Lesnek)

(RECEIVED August 27, 2019; ACCEPTED March 24, 2020)

## Abstract

Understanding marine-terminating ice sheet response to past climate transitions provides valuable long-term context for observations of modern ice sheet change. Here, we reconstruct the last deglaciation of marine-terminating Cordilleran Ice Sheet (CIS) margins in Southeast Alaska and explore potential forcings of western CIS retreat. We combine 27 new cosmogenic <sup>10</sup>Be exposure ages, 13 recently published <sup>10</sup>Be ages, and 25 new <sup>14</sup>C ages from raised marine sediments to constrain CIS recession. Retreat from the outer coast was underway by 17 ka, and the inner fjords and sounds were ice-free by 15 ka. After 15 ka, the western margin of the CIS became primarily land-terminating and alpine glaciers disappeared from the outer coast. Isolated alpine glaciers may have persisted in high inland peaks until the early Holocene. Our results suggest that the most rapid phase of CIS retreat along the Pacific coast occurred between ~17 and 15 ka. This retreat was likely driven by processes operating at the ice-ocean interface, including sea level rise and ocean warming. CIS recession after ~15 ka occurred during a time of climatic amelioration in this region, when both ocean and air temperatures increased. These data highlight the sensitivity of marine-terminating CIS regions to deglacial climate change.

**Key words:** Cordilleran Ice Sheet; <sup>10</sup>Be dating; <sup>14</sup>C dating

## INTRODUCTION

Ice sheets have surpassed glaciers and ice caps as the leading contributor to modern global sea level rise (Bamber et al., 2018), largely due to increased discharge from ice margins in contact with the ocean (i.e., marine-terminating ice sheet regions). Numerous studies have demonstrated that both oceanic and atmospheric conditions play a major role in the mass balance of marine-terminating ice sheet sectors (Joughin et al., 2012; Carr et al., 2013). However, due to the limited timescales of modern observations, the long-term (i.e., centennial-scale and longer) impact of these processes on the stability of marine-terminating ice sheet sectors is still poorly understood.

The last deglaciation is defined as the interval between the end of the global Last Glacial Maximum (LGM; ~26–19 ka; Clark et al., 2009) and the Holocene (~11.7 ka to the present; Walker et al., 2009). The last deglaciation was characterized

by overall planetary warming of several degrees and contained within it millennial-scale oscillations between warm and cold climate states, although their expressions varied spatially (Clark et al., 2012; Shakun et al., 2012). Well-constrained chronologies of ice sheet change during the last deglaciation provide key insights into the long-term controls on ice sheet behavior. Here, we reconstruct the deglaciation of a marine-terminating Cordilleran Ice Sheet (CIS) margin in coastal Southeast Alaska (Fig. 1) to improve the ice retreat chronology and to assess the impact of deglacial climate change on ice sheet stability. Previous research has demonstrated the sensitivity of land-based CIS regions to deglacial warming (Menounos et al., 2017), and several recent studies have generated direct chronologies of CIS margin retreat in Southeast Alaska and coastal British Columbia (e.g., Darvill et al., 2018; Lesnek et al., 2018). However, the causes and progression of marine-terminating CIS recession during the last deglaciation remain largely unexplored.

## REGIONAL SETTING

During the LGM, much of Southeast Alaska was covered by the CIS (Carrara et al., 2007; Lesnek et al., 2018), and at its

**Cite this article:** Lesnek, A. J., Briner, J. P., Baichtal, J. F., Lyles, A. S. 2020. New constraints on the last deglaciation of the Cordilleran Ice Sheet in coastal Southeast Alaska. *Quaternary Research* 96, 140–160. <https://doi.org/10.1017/qua.2020.32>

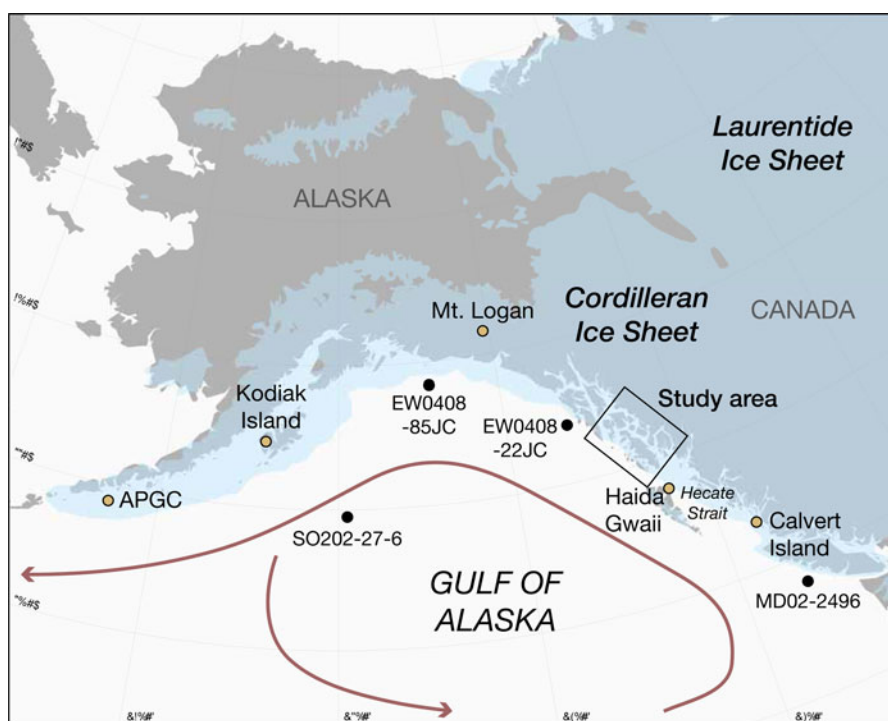


**Figure 1.** Map of the Cordilleran and Laurentide ice sheets with locations of relevant chronologies. Study area in Southeast Alaska is indicated by the black box. The approximate location and direction of the Alaska Current (Weingartner et al., 2005) is shown by the red arrows. Shaded light blue areas are ice sheet extents at  $\sim 17.3$  cal ka BP (Dyke, 2004). Black dots indicate locations of marine sediment cores: SO202-27-6 (Maier et al., 2018), EW0408-85JC (Davies et al., 2011; Praetorius and Mix, 2014; Praetorius et al., 2015), EW0408-22JC (Praetorius et al., 2016), and MD02-2946 (Cosma and Hendy, 2008; Hendy and Cosma, 2008; Taylor et al., 2014). Yellow dots indicate locations of terrestrial CIS chronology: APGC = Alaska Peninsula Glacier Complex (Misarti et al., 2012), Kodiak Island (Mann and Peteet, 1994), Mt. Logan (Fisher et al., 2008), Haida Gwaii (Clague et al., 1982; Mathewes and Clague, 2017), and Calvert Island (Darvill et al., 2018). (For interpretation of the references to color in this figure legend, the reader is referred to the web version of this article.)

maximum extent the ice sheet likely terminated somewhere on the continental shelf (Dyke, 2004; Carrara et al., 2007). Some regions along the outermost coast may have remained unglaciated during the LGM (Carrara et al., 2007), although recent evidence from  $^{10}\text{Be}$  surface exposure dating indicates that several of these hypothesized ice-free refugia were covered by the CIS (Lesnek et al., 2018). Radiocarbon-dated marine sediments suggest that the CIS reached its late Pleistocene maximum in Southeast Alaska sometime after 25 ka (Mann and Hamilton, 1995; Barrie and Conway, 1999), and Lesnek et al. (2018) combined  $^{10}\text{Be}$  and  $^{14}\text{C}$  dating to further constrain the timing of CIS maximum extent to between  $\sim 19.8$  and  $\sim 17.0$  ka in the Prince of Wales Island region. On Calvert Island (Fig. 1),  $\sim 400$  km south of the Alaskan/Canadian border, Darvill et al. (2018) found that CIS margins were in retreat by  $\sim 18.0$  ka, in agreement with minimum- and maximum-limiting  $^{14}\text{C}$  ages from Haida Gwaii (e.g., Warner et al., 1982; Mathewes and Clague, 2017). While the timing of the CIS maximum is now established at several localities along the Pacific coast, knowledge relating to post-LGM deglaciation is comparatively scarce. Radiocarbon-dated clam shells from glaciomarine mud in central Dixon Entrance sediment cores indicate deglaciation as early as  $16,650 \pm 400$  cal yr BP (Barrie and Conway, 1999). Farther south, in

Hecate Strait (Fig. 1), open water conditions by  $15,790 \pm 410$  cal yr BP have been inferred from marine sediments (Hetherington et al., 2003). Direct chronological constraints on deglaciation from terrestrial settings remain scant but suggest ice-free conditions in the easternmost portions of Southeast Alaska by the onset of the Holocene (Ives et al., 1967; Yehle, 1978; Mann, 1986; Viens, 2001; Ager et al., 2010).

Our study area is located in the southern Alexander Archipelago of Southeast Alaska (Fig. 1). The archipelago consists of more than 1000 islands, most of which reside in the Tongass National Forest. Peaks in the inland portion of the study area support local snowfields and glaciers (Fig. 2). Outer islands in the Alexander Archipelago rise from a shallow continental shelf that is crossed by deep, glacially-scoured troughs (Fig. 2). The regional climate is characterized by cool summers and mild winters, with heavy rainfall year-round. During the winter months, snow accumulation in low-elevation areas is minimal (<https://wrcc.dri.edu/summary/Climsmak.html>), but in high elevation areas, particularly among the inland mountains, snow accumulation can be more substantial. The bedrock geology of Southeast Alaska is a complex assemblage of accreted terranes of varying age, with quartz-bearing units composed of granite, granodiorite, and diorite (Wilson et al., 2015).

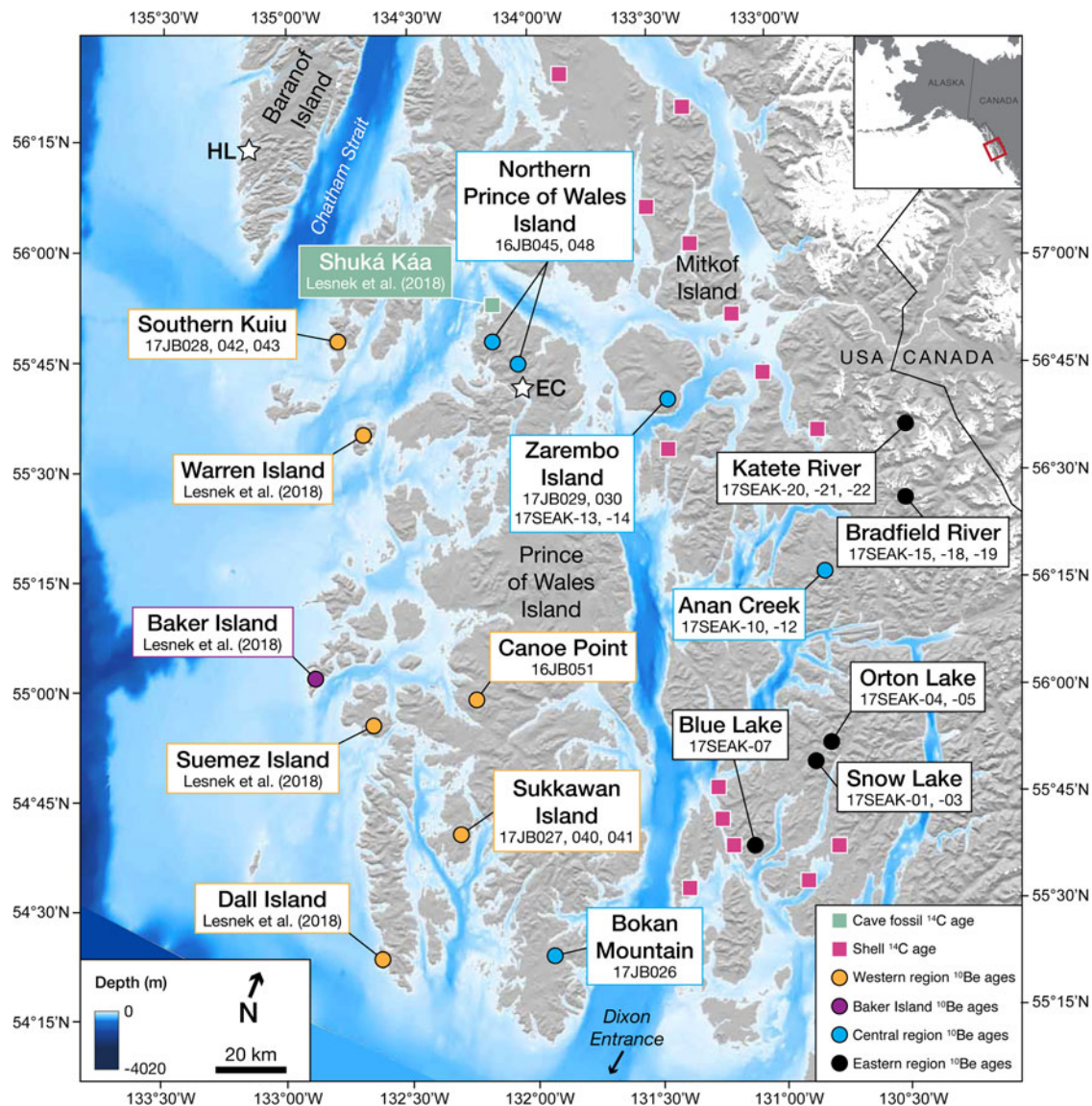


**Figure 2.** Map of study area.  $^{10}\text{Be}$  sampling sites are indicated by the dots. Sites are color coded, where yellow = western region, purple = Baker Island (local glaciers), blue = central region, and black = eastern region.  $^{14}\text{C}$  sampling locations are indicated by squares. Green = Shuká Káa cave (Lesnek et al., 2018), pink = shell-bearing raised marine sediments. White stars indicate locations of previous work mentioned in the text. HL = Hummingbird Lake (Ager et al., 2019), EC = El Capitan Cave (Wilcox et al., 2019). Modern glacier extents (white) are from version 6 of the Randolph Glacier Inventory (NSIDC, 2005, updated 2018). (For interpretation of the references to color in this figure legend, the reader is referred to the web version of this article.)

## METHODS

### $^{10}\text{Be}$ dating

#### *Sampling procedures and locations*

To directly date the timing of CIS recession, we sampled perched boulder ( $n = 24$ ) and bedrock ( $n = 3$ ) surfaces from 12 different locations in Southeast Alaska for  $^{10}\text{Be}$  exposure dating (Figs. 2 and 3). We sampled locations from the western coastline to the inland mountains with the goal of constraining deglaciation through the archipelago. Due to thick forest cover in low-lying regions, we targeted upland areas with exposed bedrock for sampling. Our sampling focused on

granitic intrusions (Wilson et al., 2015), which allowed us to obtain sufficient quartz for  $^{10}\text{Be}$  dating. We collected samples from the upper  $\sim 2$  cm of rock surfaces using a rock saw, hammer, and chisel. We recorded sample locations and elevations using a handheld GPS with  $\sim 5$  m vertical uncertainty, and we measured topographic shielding using a clinometer. In general, sampling sites were located on the unvegetated tops of bedrock ridges or the outlets of small cirques; the sites ranged in elevation from 581 to 1345 m above sea level (m asl) (Table 1), well above the local marine limit (Shugar et al., 2014; Carlson and Baichtal, 2015).

Here, we provide a more detailed description of each of the sampling sites. The first site, Southern Kuiu Island, lies just





**Figure 3.** (color online) Examples of surfaces sampled for  $^{10}\text{Be}$  dating.  $^{10}\text{Be}$  ages are shown at 1 SD internal uncertainty. See online supplemental information for photographs of all samples.

east of Chatham Strait, a deep glacially-scoured trough (Fig. 2). Samples from this site were collected from a ridge at  $\sim 650$  m asl that separates several cirques. The second site, Canoe Point, is a small ridge that sits at  $\sim 640$  m asl on central Prince of Wales Island. Our third site, Sukkawan Island, is  $\sim 3$  km off the coast of Prince of Wales Island. We collected samples at this site from a ridge on the central portion of the island that lies  $\sim 590$  m asl. At the fourth site on northern Prince of Wales Island, we collected two boulder samples on two unnamed rounded summits. These peaks are roughly 11 km south of Shuká Káa (125 m asl), an archeological site where mammal and bird bones ranging in age from more than 57 ka to modern have been excavated (Heaton and Grady, 2003; Lesnek et al., 2018). At the northern of the two summits, the boulder we sampled was perched on lichen-free bedrock at 913 m asl. At the southern peak, the sample was perched on lichen- and moss-covered bedrock.

The fifth site, Zarembo Island, sits  $\sim 40$  km east of northern Prince of Wales Island. On Zarembo Island, we sampled rock surfaces on local topographic highs. Where exposed, the bedrock on this island was somewhat lichen-covered, and the few perched boulders that we found were low lying ( $\sim 0.5$  m in height). The sixth site, Anan Creek ( $\sim 860$  m asl), is a sculpted bedrock ridge that protrudes  $\sim 100$  m above the valley floor; the exposure ages from this site record regional CIS deglaciation rather than retreat of local glaciers. Perched boulders at Anan Creek were plentiful and larger than those at other locations. Our seventh site, Bokan Mountain ( $\sim 580$  m asl), is situated on the southern tip of Prince of Wales Island. The site consisted of lichen-covered, sculpted bedrock.

The eighth site, Katete River ( $\sim 1330$  m asl), is the highest elevation site in the study region. Exposed bedrock at this site had minimal lichen cover. We sampled three boulders from a

local topographic high that protruded  $\sim 3$  m above a snowfield that was present during sampling in July 2017 (Fig. 4). Two boulders were perched on bedrock, and one boulder was perched on a field of small, potentially frost-shattered cobbles. The ninth site, Bradfield River ( $\sim 1240$  m asl), also supported a snowfield during our sampling campaign in July 2017. The three boulders sampled at this site were perched on sculpted bedrock that jutted at least 4 m above the snowfield surface (Fig. 4). The tenth site, Orton Lake, is a bedrock ridge ( $\sim 845$  m asl) surrounded by steep drops ( $>500$  m) on all sides. The bedrock at Orton Lake was ice-sculpted and had indicators of glacial erosion such as chattermarks. However, we found few large, stable perched boulders at this site; we sampled one of these boulders for  $^{10}\text{Be}$  dating. The eleventh site, Snow Lake, lies  $\sim 3$  km southwest of Orton Lake. Snow Lake is a small cirque  $<1$  km in diameter. We sampled two perched boulders near the cirque outlet. At the twelfth site, Blue Lake, we sampled one boulder on the right-lateral margin of a cirque. The cirque at Blue Lake was relatively small, and the boulder was located  $\sim 400$  m from the headwall.

#### *Quartz isolation and accelerator mass spectrometry*

Samples underwent physical and chemical preparation at the University at Buffalo Cosmogenic Isotope Laboratory using standard procedures (Kohl and Nishiizumi, 1992; Corbett et al., 2016). Samples were processed in five separate batches and spiked with  $\sim 226$ – $239$   $\mu\text{g}$  of  $^9\text{Be}$  (Table 1) using either the PRIME Lab low-level beryllium carrier (2017.11.17-Be;  $^9\text{Be}$  concentration of  $1074 \pm 8$  ppm) or the GFZ German Research Centre for Geosciences Phenakite standard ( $^9\text{Be}$  concentration of  $372.5 \pm 3.5$  ppm).

**Table 1.**  $^{10}\text{Be}$  age information.

Sample ID	Sample type	Latitude (°N)	Longitude (°W)	Elevation (m asl) <sup>†</sup>	Sample thickness (cm)	Topographic shielding correction	Quartz (g)	$^9\text{Be}$ added ( $\mu\text{g}$ )	$^{10}\text{Be}/^9\text{Be}$ ratio <sup>‡</sup>	$^{10}\text{Be}/^9\text{Be}$ ratio uncertainty	$^{10}\text{Be}$ (atoms/g)	$^{10}\text{Be}$ uncertainty (atoms/g)	$^{10}\text{Be}$ age (ka) <sup>§</sup>
<b>Western region</b>													
<i>South Kuiu</i>													
17JB028	Boulder	56.0881	134.1921	630	2.5	1.0000	17.10	226	1.48E-13	4.02E-15	1.31E + 05	3.56E + 03	17.5 ± 0.8
17JB042 <sup>+</sup>	Boulder	56.0845	134.1887	661	2.0	1.0000	19.57	226	1.15E-13	4.34E-15	8.84E + 04	3.35E + 03	11.4 ± 0.6
17JB043 <sup>+</sup>	Boulder	56.0848	134.1888	668	2.5	1.0000	29.95	228	1.96E-13	6.27E-15	9.99E + 04	3.19E + 03	12.9 ± 0.6
<i>Canoe Point</i>													
16JB051	Boulder	55.4074	132.9668	637	3.0	1.0000	11.94	239	8.01E-14	2.39E-15	1.07E + 05	3.19E + 03	16.2 ± 0.7
<i>Sukkawan Island</i>													
17JB027	Boulder	55.0881	132.7576	593	2.5	1.0000	8.87	231	6.55E-14	1.74E-15	1.14E + 05	3.03E + 03	15.9 ± 0.7
17JB040	Boulder	55.1015	132.7596	594	2.5	1.0000	11.19	233	8.68E-14	2.12E-15	1.21E + 05	2.95E + 03	16.8 ± 0.7
17JB041	Boulder	55.1023	132.7580	596	2.8	1.0000	10.69	227	8.50E-14	1.88E-15	1.21E + 05	2.67E + 03	16.8 ± 0.7
<b>Central region</b>													
<i>Northern Prince of Wales Island</i>													
16JB045	Boulder	56.2424	133.4987	913	2.5	1.0000	20.23	226	1.58E-13	3.91E-15	1.18E + 05	2.92E + 03	12.3 ± 0.5
16JB048	Boulder	56.2135	133.4331	584	4.0	1.0000	18.03	226	1.25E-13	2.42E-15	1.05E + 05	2.02E + 03	14.8 ± 0.6
<i>Zarembo Island</i>													
17JB029	Boulder	56.2914	132.7000	713	3.0	1.0000	16.07	227	1.31E-13	2.83E-15	1.23E + 05	2.67E + 03	15.4 ± 0.7
17JB030	Bedrock	56.2915	132.6999	714	2.5	1.0000	19.99	235	1.54E-13	2.90E-15	1.21E + 05	2.28E + 03	15.1 ± 0.6
17SEAK-13	Boulder	56.2910	132.6989	722	3.0	1.0000	15.11	227	9.13E-14	2.21E-15	9.15E + 04	2.21E + 03	11.3 ± 0.5
17SEAK-14 <sup>+</sup>	Bedrock	56.2905	132.6991	734	3.0	1.0000	37.17	227	2.24E-13	6.16E-15	9.14E + 04	2.51E + 03	11.2 ± 0.5
<i>Anan</i>													
17SEAK-10	Boulder	56.0764	131.7723	865	2.0	0.9986	15.02	227	1.34E-13	3.93E-15	1.35E + 05	3.97E + 03	14.8 ± 0.7
17SEAK-12	Boulder	56.0756	131.7724	851	2.5	0.9967	15.06	227	1.31E-13	2.99E-15	1.32E + 05	3.01E + 03	14.7 ± 0.6
<i>Bokan Mountain</i>													
17JB026 <sup>+</sup>	Boulder	54.9265	131.1585	581	3.3	1.0000	32.88	226	2.24E-13	6.14E-15	1.03E + 05	2.82E + 03	14.7 ± 0.7
<b>Eastern region</b>													
<i>Katete River</i>													
17SEAK-20	Boulder	56.4935	131.6732	1345	3.0	1.0000	12.09	227	7.30E-14	2.12E-15	9.17E + 04	2.67E + 03	6.8 ± 0.3
17SEAK-21	Boulder	56.4929	131.6764	1333	3.5	1.0000	12.07	227	1.09E-13	2.49E-15	1.37E + 05	3.12E + 03	10.2 ± 0.4
17SEAK-22	Boulder	56.4928	131.6765	1332	2.5	1.0000	12.07	227	1.37E-13	3.46E-15	1.72E + 05	4.35E + 03	12.8 ± 0.6
<i>Bradfield River</i>													
17SEAK-15	Boulder	56.3159	131.6115	1233	3.0	1.0000	12.13	227	5.39E-14	1.90E-15	6.73E + 04	2.37E + 03	5.5 ± 0.3
17SEAK-18	Boulder	56.3161	131.6129	1241	2.8	1.0000	12.17	227	7.99E-14	2.14E-15	9.94E + 04	2.66E + 03	7.9 ± 0.4
17SEAK-19	Boulder	56.3166	131.6136	1247	3.0	1.0000	12.11	227	6.80E-14	2.30E-15	8.53E + 04	2.88E + 03	6.8 ± 0.3
<i>Orton Lake</i>													
17SEAK-04 <sup>+</sup>	Boulder	55.6515	131.4056	840	3.0	1.0000	26.84	227	1.54E-13	4.54E-15	8.72E + 04	2.57E + 03	9.8 ± 0.5
17SEAK-05 <sup>+</sup>	Bedrock	55.6514	131.4057	850	2.0	1.0000	29.63	227	1.99E-13	6.02E-15	1.02E + 05	3.08E + 03	11.3 ± 0.5

<i>Snow Lake</i>													
17SEAK-01 <sup>+</sup>	Boulder	55.6302	131.4272	790	3.0	0.9990	19.14	227	1.28E-13	4.44E-15	1.02E+05	3.53E+03	12.0 ± 0.6
17SEAK-03 <sup>+</sup>	Boulder	55.6301	131.4286	766	2.0	0.9964	18.02	226	1.21E-13	4.95E-15	1.01E+05	4.15E+03	12.1 ± 0.5
<i>Blue Lake</i>													
17SEAK-07	Boulder	55.3626	131.5708	865	2.0	1.0000	10.19	228	6.94E-14	3.37E-15	1.04E+05	5.04E+03	11.3 ± 0.7

<sup>†</sup>Elevations and positions were recorded in the field with a Garmin handheld GPS receiver (~5 m vertical uncertainty).

<sup>‡</sup>AMS results are standardized to 07KNSTD (Nishiizumi et al., 2007); ratios are blank-corrected and shown at 1 SD uncertainty.

<sup>§</sup>Be ages reported at 1 $\sigma$  external uncertainties and calculated with version 3 of the CRONUS-Earth calculator (Balco et al., 2008) using the Arctic/Baffin Bay production rate (Young et al., 2013) and Lm scaling.

<sup>†+</sup> Measured at PRIME Lab; all other samples measured at Lawrence Livermore National Laboratory.

Accelerator mass spectrometry (AMS) was completed at Lawrence Livermore National Laboratory's Center for Accelerator Mass Spectrometry or PRIME Lab at Purdue University (Table 1). Samples measured at PRIME Lab were spiked with the PRIME Lab carrier, whereas samples measured at Lawrence Livermore National Lab were spiked with the GFZ Phenakite carrier. All sample ratios were measured with respect to the 07KNSTD standard, which has an assumed  $^{10}\text{Be}/^9\text{Be}$  ratio of  $2.85 \times 10^{-12}$  (Nishiizumi et al., 2007). Sample ratios were corrected using batch-specific blank values that ranged from  $1.17 \times 10^{-15}$  to  $3.35 \times 10^{-15}$  (average =  $2.25 \times 10^{-15}$ ;  $n = 5$ ). AMS analytical uncertainty ranged from 1.9 to 4.8%, with an average value of 2.8%.

### $^{10}\text{Be}$ age calculations and assumptions

All ages were calculated using version 3 of the online CRONUS Earth exposure age calculator (hess.ess.washington.edu; Balco et al., 2008; Balco, 2017) using the Baffin Bay/Arctic production rate (Young et al., 2013) and time-dependent (Lm) scaling (Lal, 1991). For ease of comparison with the  $^{14}\text{C}$  ages from raised marine sediments, we subtracted 67 years from the raw  $^{10}\text{Be}$  ages; thus, all  $^{10}\text{Be}$  ages are reported with respect to AD 1950.

Changes in crust elevation over a rock surface's exposure duration result in a time-varying rate of  $^{10}\text{Be}$  production. Sample elevations can be corrected for this effect using regional emergence curves, which are constrained by either glacial isostatic adjustment models or relative sea level histories (Jones et al., 2019). However, along the westernmost coast of Southeast Alaska, relative sea level history in the early deglacial period is largely unconstrained (Shugar et al., 2014). A wave-cut terrace at ~165 m below sea level may correlate with a late Pleistocene lowstand (Carlson, 2007), but this feature is undated. The migration of a crustal forebulge (Carlson and Baichtal, 2015) through the outer islands of Southeast Alaska likely caused a relative sea level rise until ~10.6 ka, reaching a maximum of 25 m asl, followed by sea level fall to the present (Baichtal and Carlson, 2010). Farther inland, land surfaces experienced net isostatic uplift (i.e., relative sea level fall) following deglaciation, with a maximum elevation change of 191 m since ~13.7 ka. In addition, atmospheric compression above a sample site that has moved up or down in elevation, and shifts in the air pressure field due to a site's proximity to the ice margin, may counteract the effects of isostatic rebound on  $^{10}\text{Be}$  production rates (Staiger et al., 2007). Due to (1) the variable and unconstrained nature of relative sea level change in this region, (2) the potential effects of changing atmospheric pressure through time at our sampling sites, and because (3) the production rate calibration dataset used to calculate our ages was not corrected for isostatic adjustment (Young et al., 2013), we report our  $^{10}\text{Be}$  ages without elevation corrections.

We made no corrections for post-depositional erosion. We observed pristine, glacially-scoured surfaces on bedrock adjacent to our perched boulder samples, suggesting minimal surface erosion since deglaciation. Extended intervals of thick



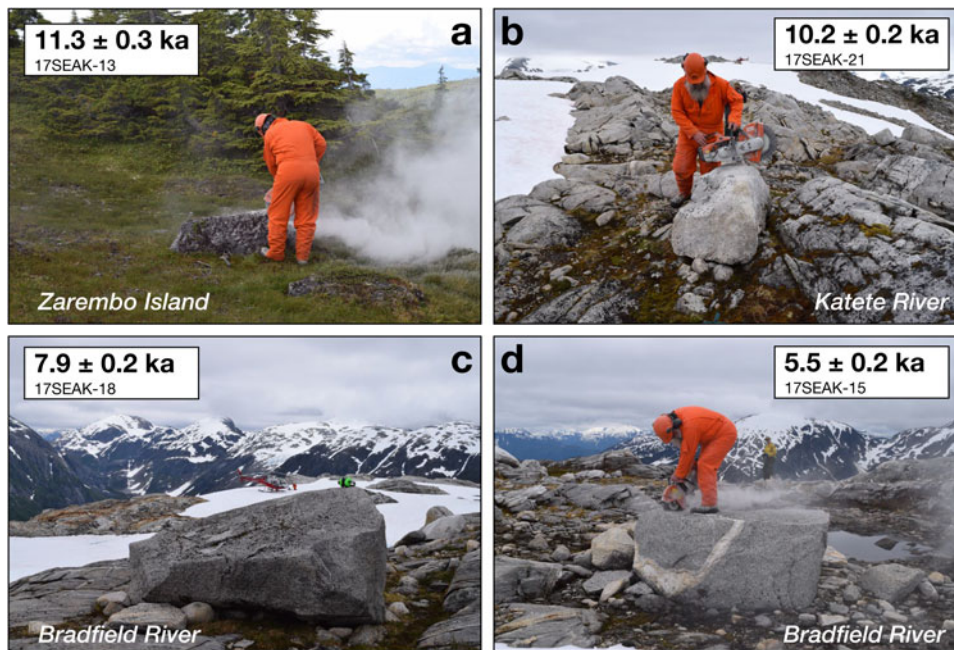


**Figure 4.** (color online) Samples with  $^{10}\text{Be}$  ages that are potentially impacted by snow shielding. Photos were taken during field work in July 2017. All  $^{10}\text{Be}$  ages are shown at 1 SD internal uncertainty. (A) Boulder from Zarembo Island. The boulder surface is lichen-covered, but the boulder is less than 1 m in height. (B) Boulder from the Katete River site. Note the largely lichen-free surface and snow field in the background. Sample is  $\sim 3$  m above the snow surface. (C–D) Boulders from the Bradfield River site. The boulders are large and appear to be stable, but the lack of lichen on their surfaces may be indicative of seasonal snow cover. Samples are  $\sim 4$  m above the snowfield surface.

snow cover over a rock surface can lead to erroneously young apparent exposure ages. Modern snowfall data (since the 1940s) from the Western Regional Climate Center (<https://wrcc.dri.edu/summary/Climsmak.html>) indicates that most of the low-lying regions in Southeast Alaska have an average wintertime snow depth of fewer than 10 to 20 centimeters. It is likely that our high elevation sampling sites experienced more snow cover than the weather stations referenced above (see Discussion). However, the lack of snowfall data for these regions leads us to report our exposure ages without snow shielding corrections. Therefore, the  $^{10}\text{Be}$  ages reported here should be viewed as minimum exposure ages.

When interpreting  $^{10}\text{Be}$  surface exposure ages, an important consideration is the erosional capacity of the overriding ice. Overriding by weakly or non-erosive (i.e., cold-based) ice allows accumulated isotopes from previous exposure periods to remain in a surface (Bierman et al., 1999; Corbett et al., 2013). To test for isotopic inheritance in our study area, we measured  $^{10}\text{Be}$  concentrations in adjacent boulder and bedrock surfaces.

### $^{14}\text{C}$ dating

An extensive literature search and years of field reconnaissance have resulted in a dataset of over 620 shell-bearing raised marine deposits throughout Southeast Alaska. A select subset of this data is reported here. Samples of shell-bearing strata were found in various locations across the islands of Southeast Alaska. We collected material from raised marine deposits at 25 sites across the study area (Fig. 2) following

the procedures outlined in Carlson and Baichtal (2015). Many sites were exposed during road, quarry, or building excavations. Some are from deposits exposed in landslides, river and creek beds, or along wave-cut shorelines. In general, the deposits were stratified (Fig. 5), and where possible, samples were collected from multiple layers within the same set of sediments. Elevation measurements were taken using hand-held barometric digital altimeters accurate to  $\pm 1$  m and were zeroed twice daily. When possible, LiDAR-generated data points were averaged to obtain elevations or to create a local datum. All elevations were calculated relative to mean lower low water (MLLW), measured multiple times, and averaged. Subsequently, some elevations were verified from LiDAR data acquired in 2017 and 2018.

Bulk samples were taken of the shell materials and carried from the field in gallon-sized resealable plastic bags. Recovered samples were washed and screened through two graduated U.S.A. Standard Testing Sieves, #16, 1.18 microns (0.0469 inches) and #200, 0.075 microns (0.0029 inches). Samples were air-dried. Large shells, bone and wood samples were separated out for identification to genus and species when possible. The finer sediment was examined under varying magnification and handpicked for shell, fish bone, charcoal, wood and plant fragments, foraminifera, ostracods, and otoliths and identified to genus and species when possible. To ensure that that long-lived shell species would not bias the dating process, fragments of small shells, gastropods, and barnacle plates were selected for dating. Because living clams can burrow through sediment to a great depth, effectively burrowing into older strata, paired valves in growth position were

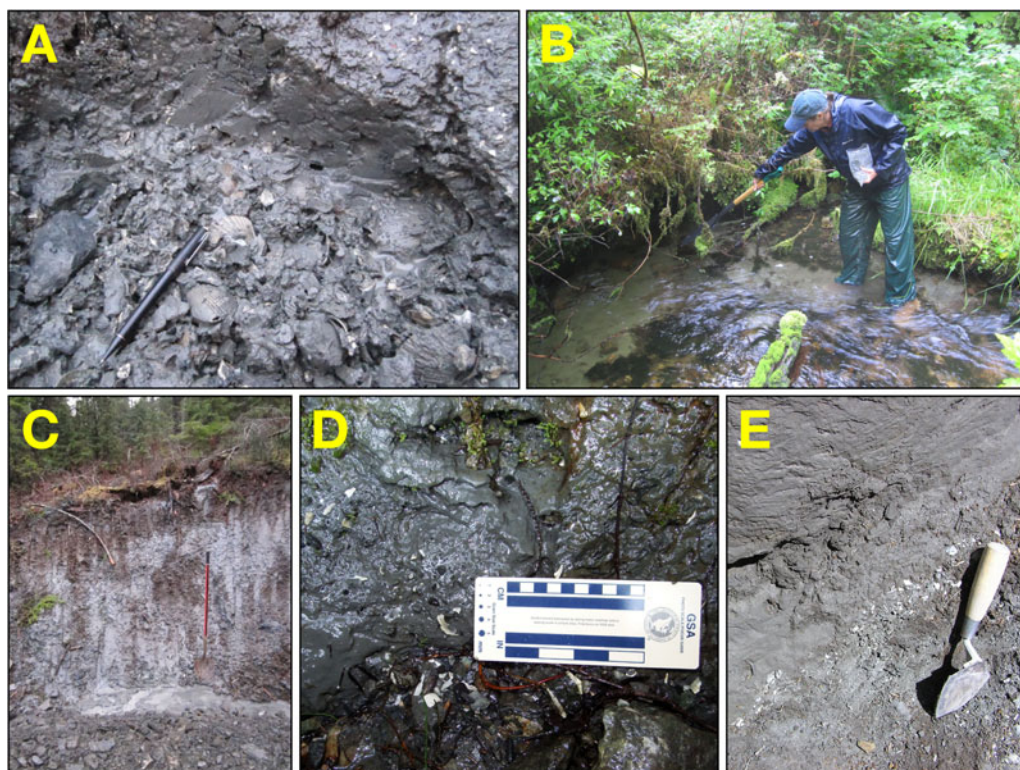


**Figure 5.** (color online) Representative raised marine sediments and samples for  $^{14}\text{C}$  dating. (A) Shells embedded in raised marine sediments on Mitkof Island. (B) Marine sediments on Wrangell Island. (C) Section of raised marine sediments from Kupreanof Island. (D) Shells from Gravina Island. (E) Section of raised marine sediments on Revillagigedo Island.

not dated. However, samples of paired valves in growth position were collected for species identification. We also collected barnacles and serpulid worm casts for dating (Table 2). In all, these invertebrates are generally found in the intertidal to subtidal zones, and provide closely-limiting constraints on sea level, and therefore CIS retreat.

Samples were prepared for AMS measurements at the Beta Analytic laboratory or the USGS  $^{14}\text{C}$  Laboratory, and  $^{14}\text{C}$  measurements were completed at Beta Analytic or Lawrence Livermore National Laboratory. We corrected shell ages using a locally calibrated marine reservoir age, where  $\Delta R$  is 700 years (total reservoir correction = 1100 years; Josenhans et al., 1997; Addison et al., 2010). Ages were calculated in OxCal version 4.3 (Bronk Ramsey, 2009) using the Marine13 calibration curve (Reimer et al., 2013), and are shown at two standard deviation (2 SD) uncertainty.

### Ice flow mapping

To reconstruct CIS flow direction, we identified and mapped glacial flow indicators across coastal Southeast Alaska through a combination of field reconnaissance and remote sensing. Throughout the study area, we measured the direction of 231 striations in the field using a handheld compass. We also identified land-based ice flow indicators such as drumlins and crag and tail features using publicly available LiDAR Digital Terrain Models (DTMs) for Prince of Wales Island from the Alaska Division of Geological and

Geophysical Surveys (<https://elevation.alaska.gov>). The LiDAR surveys were flown in 2017 and the resulting DTMs have a vertical accuracy of 19.6 cm or better at the 95% confidence interval. We created hillshade maps of Prince of Wales Island using an illumination azimuth and inclination of  $315^\circ$  and  $30^\circ$ , respectively. In addition, we mapped streamlined bedforms, such as drumlins and megascale glacial lineations, on the seafloor using Bathymetric Attributed Grid (BAG) shaded relief maps downloaded from the NOAA National Centers for Climate Information (<https://maps.ngdc.noaa.gov/viewers/bathymetry/>).

## RESULTS

### $^{10}\text{Be}$ ages

All  $^{10}\text{Be}$  ages are discussed in the following paragraphs are presented in Figure 6. Normalized kernel density estimates for each site are shown in Figures 7 through 9, and Figure 10 shows combined normalized kernel density estimates. All  $^{10}\text{Be}$  ages reported at 1 SD external uncertainty, which includes production rate uncertainty.

On southern Kuiu Island, exposure ages from three perched boulders are  $17.5 \pm 0.8$ ,  $12.9 \pm 0.6$ , and  $11.4 \pm 0.6$  ka. At Canoe Point on west central Prince of Wales Island, a perched boulder yields an exposure age of  $16.2 \pm 0.7$  ka. On Sukkawan Island, west of Prince of Wales Island, three perched boulders have exposure ages of  $15.9 \pm 0.7$ ,  $16.8 \pm 0.7$ , and  $16.8 \pm 0.7$  ka.



**Table 2.**  $^{14}\text{C}$  age information.

Field ID	Lab ID	Latitude (°N)	Longitude (°W)	Elevation (m asl)	Material dated	$\delta^{13}\text{C}$ (‰)	$\Delta\text{R}$ (yr)	$\Delta\text{R}$ uncertainty (yr)	$^{14}\text{C}$ age (yr)	$^{14}\text{C}$ uncertainty (yr)	Calibrated age (cal yr BP)	Calibrated uncertainty (yr)
ETOLIN1	Beta - 145936	56.187	-132.630	37.1	<i>Macoma nasuta</i>	0.0	300	80	12540	180	13720	420
GRAVINA2	Beta - 143082	55.187	-131.730	2.0	<i>Nuculana minuta</i>	0	300	80	13720	90	15580	370
GRAVINA6	Beta - 472318	55.186	-131.729	6.0	<i>Hiatella arctica</i>	1.6	300	80	13110	40	14550	430
GRAVINA7	Beta - 472319	55.191	-131.728	6.0	<i>Nuculana minuta</i>	0.3	300	80	13350	40	14920	390
KUPRE1	Beta - 145932	57.000	-133.143	41.1	<i>Balanus</i> sp. fragments	0	300	80	12440	120	13610	300
KUPRE2	Beta - 145930	57.000	-133.216	30.0	<i>Balanus</i> sp. fragments	-0.7	300	80	13270	50	14750	440
KUPRE3	Beta - 145931	57.000	-133.216	30.0	<i>Balanus</i> sp. fragments	1.1	300	80	13230	40	14700	430
KUPRE10	Beta - 357132	56.943	-133.840	80.0	<i>Saxidomus gigantea</i>	-0.1	300	80	13180	50	14640	440
KUPRE11	Beta - 357142	56.721	-133.172	44.0	<i>Saxidomus gigantea</i> and <i>malcoma</i> sp. fragments	-0.4	300	80	13210	50	14680	440
KUPRE13	Beta - 395240	56.714	-132.957	39.6	<i>Hiatella arctica</i> and <i>Saxidomus gigantea</i> fragments	-0.4	300	80	13030	40	14420	410
MAIN6	Beta - 357145	56.370	-132.035	10.7	<i>Nuculana minuta</i>	-0.1	300	80	13130	50	14580	440
MITKOF8	Beta - 307866	56.689	-132.910	46.1	<i>Saxidomus gigantea</i>	0.6	300	80	13240	60	14710	450
MITKOF11	Beta - 307875	56.570	-132.580	12.1	<i>Balanus</i> sp. fragments	0.4	300	80	12720	50	13900	230
MITKOF12	Beta - 307874	56.558	-132.620	25.1	<i>Balanus</i> sp. fragments	-0.2	300	80	12550	50	13700	230
MITKOF13	Beta - 307873	56.558	-132.620	24.1	<i>Balanus</i> sp. fragments	-0.5	300	80	12880	50	14130	330
MITKOF15	Beta - 418060	56.711	-132.937	39.0	<i>Hiatella arctica</i>	0.4	300	80	13020	40	14400	400
REVILLA4	Beta - 129418	55.337	-131.630	12.1	<i>Balanus</i> sp. and <i>Serpula</i> sp. fragments	0	300	80	12640	90	13800	290
REVILLA5	Beta - 53214	55.337	-131.631	21.3	<i>Balanus</i> sp. and <i>Serpula</i> sp. fragments	-	300	80	12710	70	13880	260
REVILLA7	Beta - 145934	55.343	-131.273	54.3	<i>Macoma nasuta</i>	-0.2	300	80	13070	80	14520	470

REVILLA8	Beta - 129420	55.389	-131.734	24.4	<i>Balanus</i> sp. and <i>Serpula</i> sp.fragments	0	300	80	13440	370	15050	1140
REVILLA9	Beta - 129419	55.389	-131.735	21.0	<i>Balanus</i> sp. and <i>Serpula</i> sp.fragments	0	300	80	12800	240	14220	770
REVILLA10	WW-2381	55.429	-131.785	30.8	<i>Niculana minuta</i>	-	300	80	13050	50	14460	430
REVILLA12	WW-2382	55.445	-131.805	53.7	<i>Niculana minuta</i>	-	300	80	13430	50	15110	380
REVILLA16	Beta - 246551	55.425	-131.250	78.5	<i>Balanus</i> sp. fragments	0	300	80	13030	50	14430	420
WGL5	Beta - 307864	56.473	-132.382	36.0	<i>Chlamys</i> sp.	0.6	300	80	13060	50	14480	430

Combined with nine <sup>10</sup>Be ages previously reported by Lesnek et al. (2018), the average exposure age for this outer region is 16.9 ± 0.6 ka (mean ± 1 SD; n = 12; Fig. 7). This average excludes three outliers, which fall more than 2 SD outside of the mean (15SEAK-12, 17JB042, 17JB043; Table 1).

On northern Prince of Wales Island, two boulders have exposure ages of 14.8 ± 0.5 and 12.3 ± 0.5 ka. On Zarembo Island, two perched boulders yield exposure ages of 15.4 ± 0.7 and 11.3 ± 0.5 ka, and two bedrock surfaces have exposure ages of 15.1 ± 0.6 and 11.3 ± 0.2 ka. At Anan Creek, two boulders yield <sup>10</sup>Be ages of 14.7 ± 0.6 and 14.8 ± 0.7 ka. Finally, at Bokan Mountain on southern Prince of Wales Island, one perched boulder has an exposure age of 14.7 ± 0.7 ka. Although these four sites are separated by as much as 150 km in the north-south direction, we find no trend in age across the region; we therefore average all the <sup>10</sup>Be ages for the central region. Excluding three young outliers whose ages fall more than 2 SD outside the mean of the population (16JB045, 17SEAK-13, 17SEAK-14; Table 1), the <sup>10</sup>Be ages average 14.9 ± 0.3 ka (mean ± 1 SD; n = 6; Fig. 8).

At the Katete River site (~1335 m asl), three boulder ages have exposure ages of 12.8 ± 0.6, 10.2 ± 0.4, and 6.8 ± 0.3 ka. At the Bradfield River site (~1240 m asl), three boulders perched directly on bedrock or smaller clasts on bedrock yield <sup>10</sup>Be ages of 7.9 ± 0.4, 6.8 ± 0.3, and 5.5 ± 0.3 ka. At Orton Lake, we sampled a perched boulder and the upper surface of a sculpted bedrock ridge. The boulder has a <sup>10</sup>Be age of 9.8 ± 0.5 ka, whereas the sculpted bedrock has a <sup>10</sup>Be age of 11.3 ± 0.5 ka. At Snow Lake, two boulders in a small cirque yield ages of 12.1 ± 0.5 and 12.0 ± 0.6 ka. At Blue Lake, one perched boulder on the right-lateral margin of a small cirque has an exposure age of 11.3 ± 0.7 ka.

### <sup>14</sup>C ages

The dated materials from raised marine deposits across the field area (Figs. 5 and 6) provide minimum-limiting constraints on CIS deglaciation. The elevations of these deposits are not consistent across the study area; this variability is due to differential isostatic uplift since deglaciation. The ages range from 13,610 ± 300 to 15,580 ± 370 cal yr BP (n = 25), and there is no spatially coherent pattern with age.

### CIS extent and flow direction

Based on our <sup>10</sup>Be dating in the western region (this study; Lesnek et al., 2018) and seafloor geomorphology (see Methods), we reconstructed the maximum extent of the CIS during the latest Pleistocene (Fig. 11). Previously published chronology indicates that CIS maximum extent was achieved between ~20 and 17 ka (Lesnek et al., 2018). This updated mapping builds on work published by Carrara et al. (2007), who identified several areas along the western coast of Southeast Alaska that may have served as ice-free refugia during the LGM. In our refined reconstruction (Fig. 11), Dall, Suemez, and Warren Islands, which were listed as potential refugia by Carrara et al. (2007), are covered by ice during the CIS

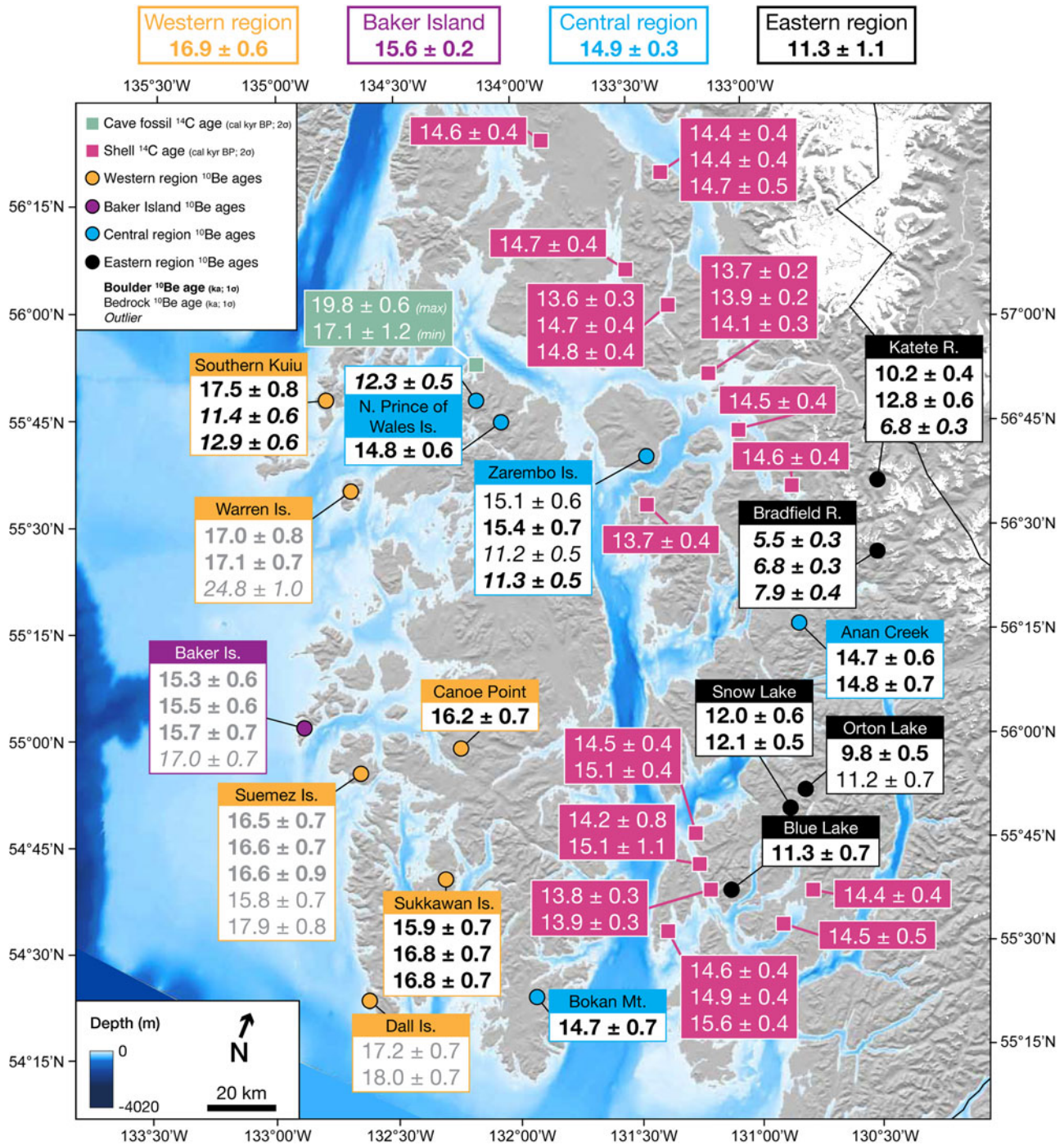


**Figure 6.** Map of Southeast Alaska with deglaciation chronology. Ages are color coded by type and region. <sup>14</sup>C ages from Shuká Káa (Lesnek et al., 2018) are shown in green boxes with white text. Minimum-limiting <sup>14</sup>C ages from raised marine sediments are shown in pink boxes with white text. All <sup>14</sup>C ages are calibrated and shown at 2 SD uncertainty. <sup>10</sup>Be ages from this study are shown in white boxes with black text. Previously published <sup>10</sup>Be ages (Lesnek et al., 2018) are indicated with gray text. Boulder ages are in bold text, bedrock ages are in normal text. All <sup>10</sup>Be ages are color coded by region: yellow = western region, purple = Baker Island (local glaciers), blue = central region, and black = eastern region. Outliers are indicated by italic text. All <sup>10</sup>Be ages are shown at 1 SD external uncertainty. Average <sup>10</sup>Be ages for each region (mean ± 1 SD) are shown at the top of the image. (For interpretation of the references to color in this figure legend, the reader is referred to the web version of this article.)

maximum stage because <sup>10</sup>Be ages from these islands indicate deglaciation at ~17 ka (this study; Lesnek et al., 2018). However, because we do not have exposure ages from other locations identified as potential refugia by Carrara et al.

(2007), including portions of Baranof, Coronation, Noyes, Baker, and Forrester islands, we cannot rule out the possibility that those locations escaped cover by the CIS (but perhaps not local glaciers) during the regional LGM (Fig. 11). As



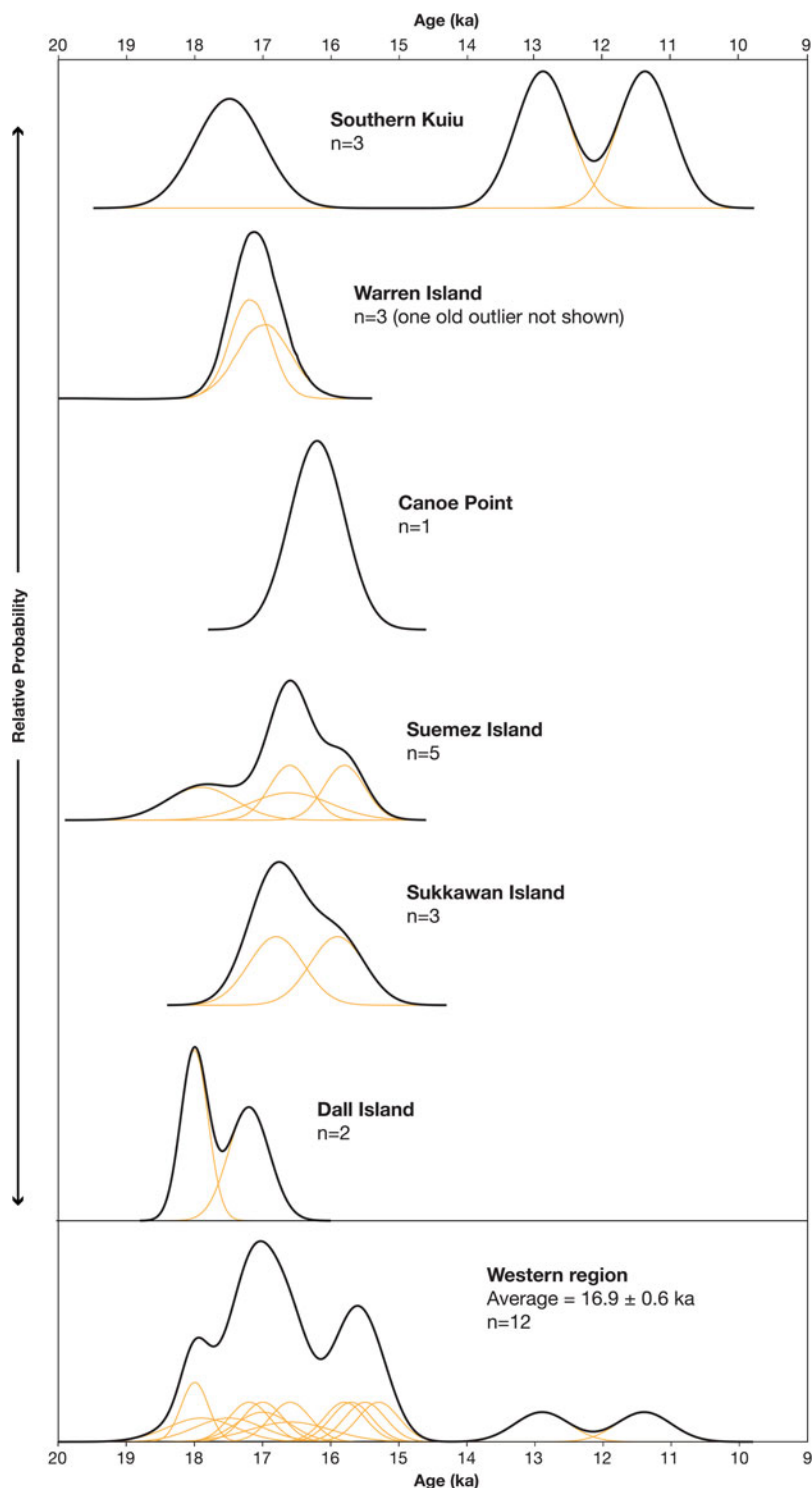


**Figure 7.** (color online) Normalized kernel density estimates for  $^{10}\text{Be}$  ages in the western region of the study area. All  $^{10}\text{Be}$  ages are plotted with 1 SD internal uncertainty. In the bottom panel, all ages from the western region are summed, and the average age for the western region group excludes three outliers (two young outliers, one old outlier that is not pictured) that were 2 SD outside of the mean.

such, in this updated reconstruction, we follow the original interpretations of Carrara et al. (2007) and leave these areas ice-free. While the ice extent map presented here is an improvement on previous work, we emphasize that this new map is largely speculative, and needs to be further refined with chronology from the potential refugia.

LiDAR-based Digital Evaluation Models (DEMs) of Prince of Wales Island reveal hundreds of ice flow indicators, including crag and tail features ( $n = 336$ ) and drumlins ( $n = 1249$ ). These features vary in both size and density on the landscape, with the largest and most concentrated occurrences appearing on the eastern side of Prince of Wales

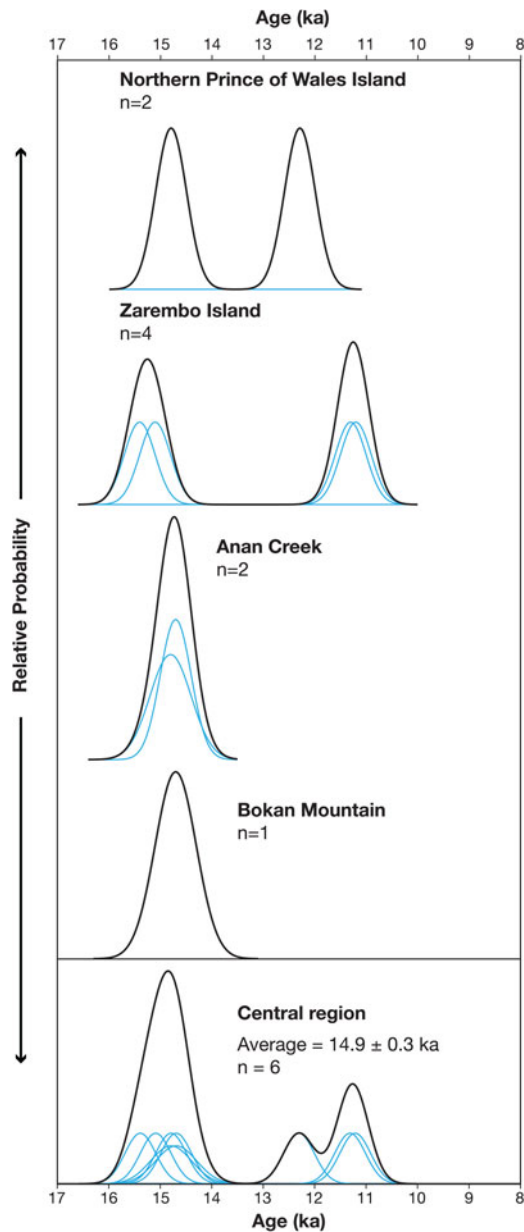


**Figure 8.** (color online) Normalized kernel density estimates for  $^{10}\text{Be}$  ages in the central region of the study area. All  $^{10}\text{Be}$  ages are plotted with 1 SD internal uncertainty. In the bottom panel, all ages from the central region are summed, and the average age for the central region excludes three young outliers.

Island, flowing into Clarence Strait (see online supplemental material). We also used striations preserved on bedrock to infer flow direction throughout the study region (Fig. 11). In some cases, striations close to one another are not parallel, suggesting either complex local flow during the last glacial period or multiple phases of ice flow during deglaciation. Additionally, streamlined bedforms up to 5 km in length are found on the seafloor in Clarence, Sumner, and Chatham straits (Fig. 11). These bedforms generally follow topography, and may be indicative of grounded ice streams during the LGM (Eyles et al., 2018).

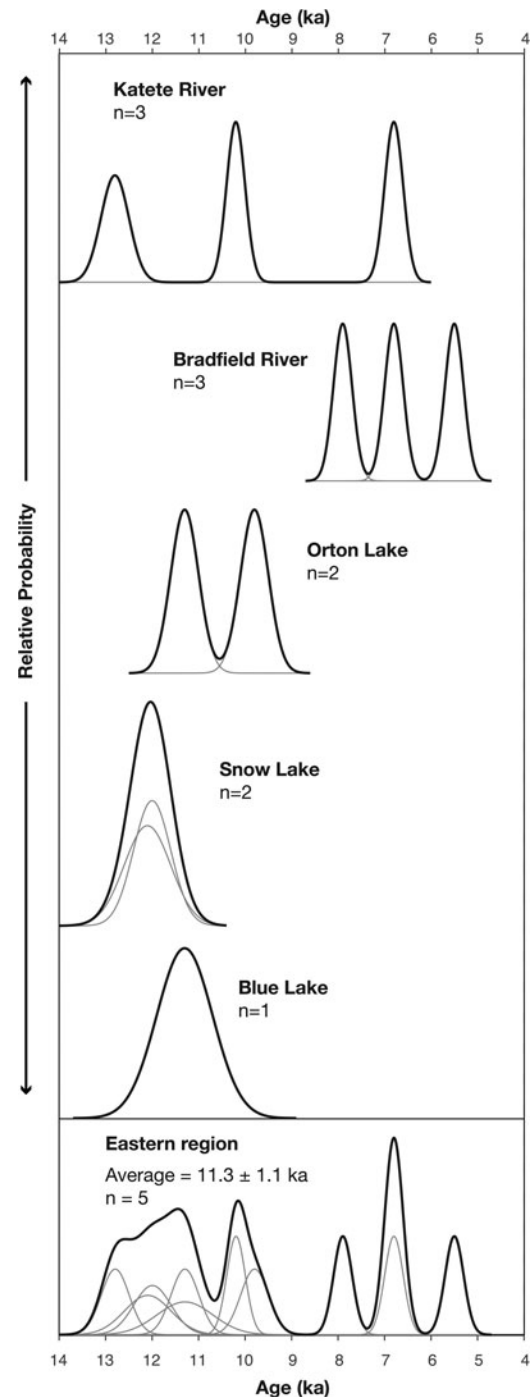


**Figure 9.** Normalized kernel density estimates for  $^{10}\text{Be}$  ages in the eastern region of the study area. In the bottom panel, all ages from the eastern region are summed, and the average age for the eastern region excludes six young outliers.

## DISCUSSION

### Chronology of Cordilleran Ice Sheet retreat in Southeast Alaska

Based on the clustering of  $^{10}\text{Be}$  ages across the study area (Fig. 10), we have grouped the sites into three distinct phases of glacial retreat. The first group, which we term the “western

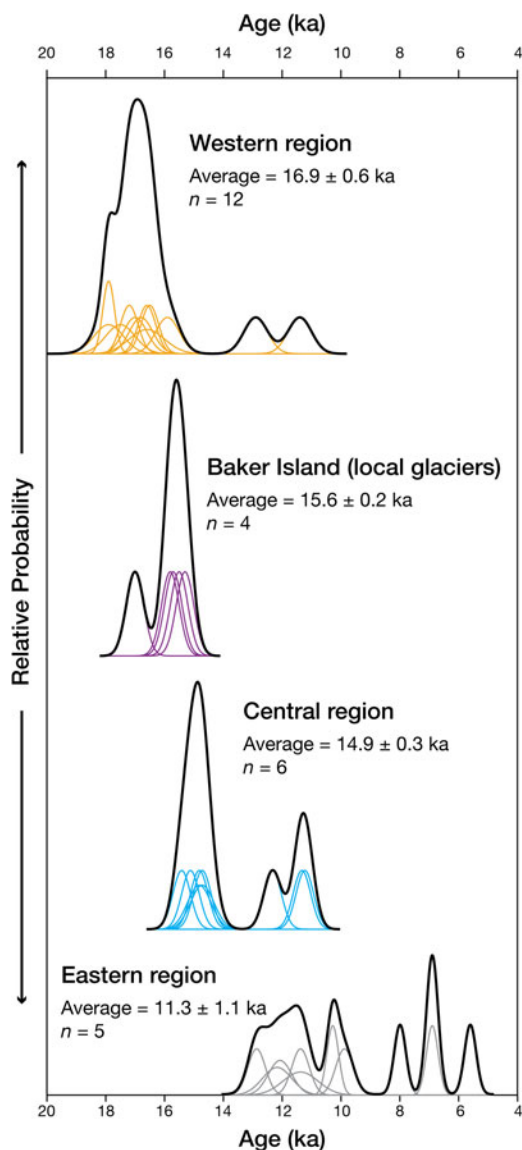


**Figure 10.** (color online) Normalized kernel density estimates for  $^{10}\text{Be}$  ages in all regions in the study area, including Baker Island.

region,” encompasses sites that date the initial retreat of the CIS from what is now the westernmost coast of Southeast Alaska. The second group, termed the “central region,” is composed of sites that track CIS recession through the fjords in Southeast Alaska. The last group, the “eastern region,” consists of cirque floors or ridgetops between cirques that date the final retreat of small glaciers independent of the CIS.

Our  $^{10}\text{Be}$  ages from perched boulders and bedrock in the western region place ice retreat from the outer islands of the Alexander Archipelago at  $16.9 \pm 0.6$  ka (mean  $\pm 1$  SD;  $n = 12$ ). The anomalously old exposure age from bedrock on Warren Island (15SEAK-12;  $24.8 \pm 1.0$  ka) is likely due to inherited  $^{10}\text{Be}$  that accumulated prior to the most recent deglaciation and was previously discussed in Lesnek et al. (2018). We identified two young outliers at the Southern Kuiu Island site: one perched boulder (17JB042;  $11.4 \pm 0.6$  ka; boulder height  $\sim 1.25$  m) and one bedrock sample

(17JB043;  $12.9 \pm 0.6$  ka). The coastal location of the site, the lichen-covered boulder surface, and the sample elevation ( $\sim 665$  m asl) suggest that in modern times, the site does not experience much snow accumulation during the winter months. A 1.5-m-tall perched boulder  $\sim 400$  m north of the above samples returned an exposure age of  $17.5 \pm 0.8$  ka, which aligns well with  $^{10}\text{Be}$  ages from other perched boulders and bedrock in our western region (Lesnek et al., 2018).

The  $^{10}\text{Be}$  ages from the central region of the study area suggest the CIS evacuated the fjords in coastal Southeast Alaska by  $14.9 \pm 0.3$  ka (mean  $\pm 1$  SD;  $n = 6$ ). This average excludes three ages from two locations in the central region: northern Prince of Wales Island and Zarembo Island. The age of  $12.3 \pm 0.5$  ka from a boulder on northern Prince of Wales Island (Fig. 6; 16JB045) may be too young due to sediment shielding, or perhaps snow shielding as the sample lies at a relatively high elevation of 913 m asl. The  $^{10}\text{Be}$  ages from Zarembo Island are more difficult to interpret. We collected two boulder-bedrock pairs at this site, and one pair returned ages of  $\sim 15.3$  ka while the other pair yielded exposure ages of  $\sim 11.3$  ka (Fig. 6). The boulder-bedrock pairs come from similar locations, and are separated by fewer than 100 m laterally. The younger ages are from a slightly higher elevation ( $\sim 730$  vs.  $\sim 713$  m asl). The two boulders collected from this site are also similar in height and their degree of lichen cover, and both boulders were perched on vegetated (currently stable) bedrock. From this site alone, it would be challenging to determine which of the two boulder-bedrock pairs more accurately dates the timing of CIS retreat. However,  $^{10}\text{Be}$  ages from elsewhere in the central region and the minimum-limiting  $^{14}\text{C}$  ages from raised marine sediments (Fig. 6) suggest the CIS had evacuated southern Southeast Alaska’s fjords sometime between  $\sim 15.6$  and  $13.6$  cal ka BP. This interpretation is supported by previous work in the region; for example, radiocarbon-dated marine sediments suggest the outlet glacier occupying Dixon Entrance (Fig. 2) had receded to the modern coastline by  $\sim 14.5$  cal ka BP (Barrie and Conway, 1999). Additionally, on southwestern Baranof Island (Fig. 2),  $^{14}\text{C}$ -dated lake sediments suggest ice-free conditions by  $\sim 14.6$  cal ka BP (Ager, 2019). In all, the available chronology suggests that the  $\sim 15.3$  ka ages on Zarembo Island are more likely accurately dating regional deglaciation than the  $\sim 11.3$  ka ages. Thus, the older ages from Zarembo Island are included in the regional average  $^{10}\text{Be}$  age of  $14.9 \pm 0.3$  ka (mean  $\pm 1$  SD;  $n = 6$ ).

The  $^{10}\text{Be}$  ages from inland cirques and ridges are more scattered than those from the other two regions (Figs. 6 and 9), and consequently definitive interpretations are more difficult to make. Scatter in the exposure ages is particularly apparent at the Bradfield River and Katete River sites, which are both situated  $>1200$  m asl. These sites host snowfields that persisted through the summer in 2017 (Fig. 4). Boulders at these sites lacked significant lichen cover on their surfaces, suggesting that even under modern climatic conditions, they retain persistent snow cover throughout most of the year. Thus, the  $^{10}\text{Be}$  ages from the Bradfield and Katete river sites should strictly be viewed as minima.



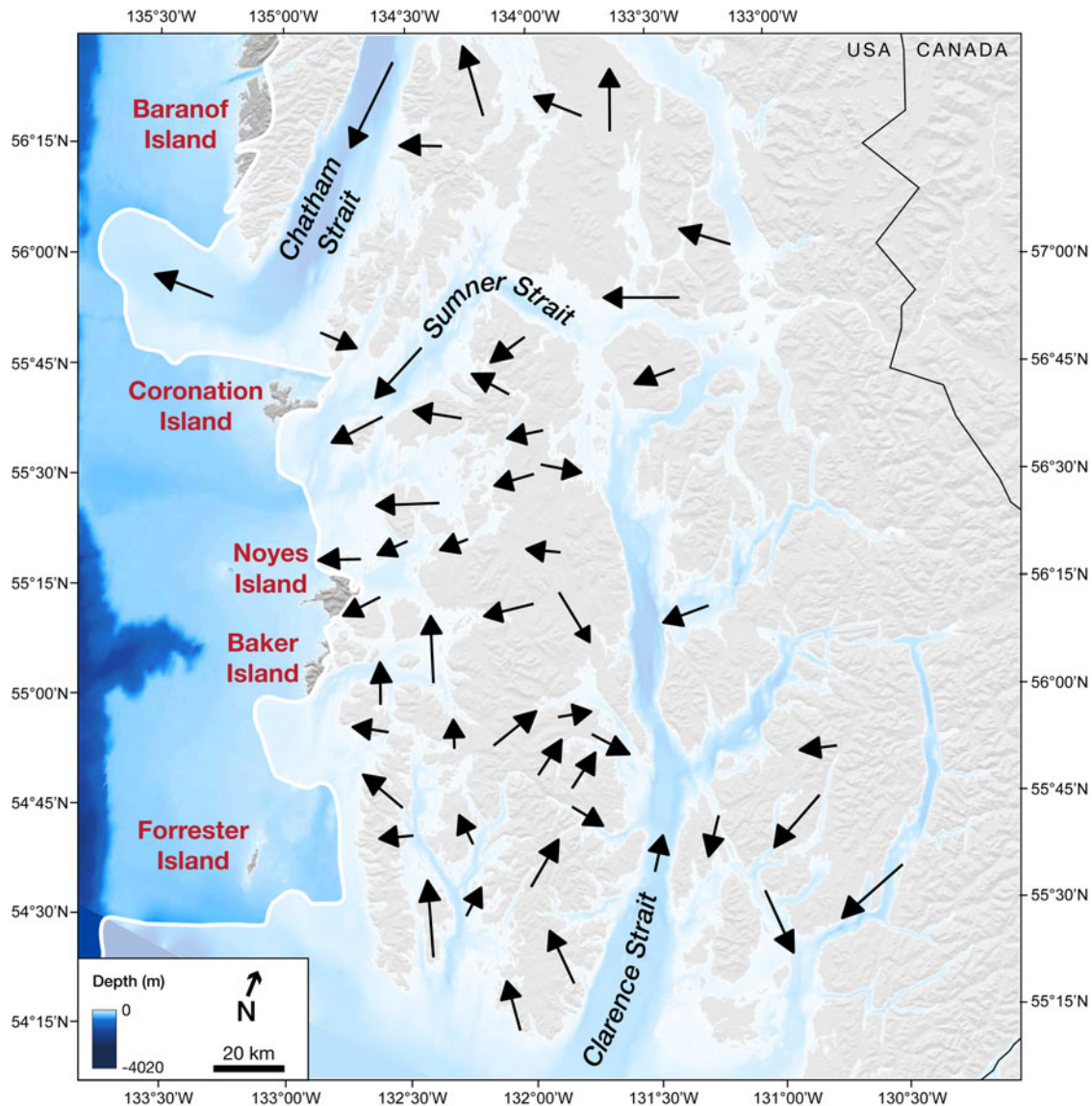


**Figure 11.** Map of inferred CIS maximum extent ( $\sim 20$ – $17$  ka) and flow direction during the latest Pleistocene. CIS extent (white lines and shading) is updated from Carrara et al. (2007) and inferred from  $^{10}\text{Be}$  ages in the western region of the study area and bathymetry. Ice-free refugia may have existed on Baranof, Coronation, Noyes, Baker, and Forrester islands (red text). Black arrows represent average ice flow based on groups of at least five directional indicators, such as striations, drumlins, and crag and tails. For additional details on the ice flow indicators, we direct the reader to the online supplementary information. (For interpretation of the references to color in this figure legend, the reader is referred to the web version of this article.)

Ages from the southern sites in the eastern region (Orton, Snow, and Blue lakes) are more coherent; samples are from lower elevations and field evidence is less consistent with persistent snow cover. Samples from Orton, Snow, and Blue lakes return exposure ages that average  $11.3 \pm 1.1$  ka (mean  $\pm 1$  SD;  $n = 5$ ). This age for deglaciation at these sites is supported by  $^{36}\text{Cl}$  exposure ages from glacially-abraded bedrock on the summit of Mitkof Island (Fig. 2), which indicate deglaciation by  $\sim 11.3$  ka (Viens, 2001). In aggregate, our results from the eastern region suggest that local glaciers were probably present in the southern Southeast Alaskan Coast Mountains until at least the early Holocene.

In all three regions of the study area, we find surfaces with early Holocene exposure ages (Fig. 10). At one site in the western region (Southern Kuiu Island) and two sites in the central region (northern Prince of Wales Island and Zarembo Island), these surfaces are several thousand years younger than the mean deglaciation age, which is  $16.9 \pm 0.6$  ka and  $14.9 \pm 0.3$  ka, respectively. When combined with  $^{10}\text{Be}$  ages from the eastern region, these samples average  $11.5 \pm 0.9$  ka ( $n = 12$ ). The clustering of ages about this mean, at sites that are separated in some cases by more than 150 km, suggests these ages may have climatic significance, which we discuss further below.

## Cordilleran Ice Sheet deglaciation across the North Pacific

Our results are consistent with previously published reconstructions from other marine-terminating CIS margins along the North Pacific coast, implying that broad regions of the ice sheet behaved synchronously during deglaciation. Our ages from the western region suggest that initial CIS retreat was underway by  $\sim 17$  ka. Immediately to the south of our study area,  $^{14}\text{C}$  ages from Haida Gwaii and nearby Hecate Strait (Fig. 1) suggest the CIS may have been retreating as early as  $\sim 19$  ka (Clague et al., 1982; Blaise et al., 1990; Mathewes and Clague, 2017). Farther south,  $^{10}\text{Be}$  ages from Calvert Island (Fig. 1) suggest that the CIS had retreated to the modern coastline at  $\sim 18$  ka (Darvill et al., 2018). Similarly, terrestrial  $^{14}\text{C}$  ages from Kodiak Island, southern Alaska (Mann and Peteet, 1994), and the Alaska Peninsula Glacier Complex (Misarti et al., 2012) indicate initial glacier retreat  $\sim 17$  ka (Fig. 1). Ice-rafted debris records from the Southeast Alaska margin (Praetorius et al., 2016), the Vancouver Island shelf (Fig. 12g; Cosma et al., 2008), and the coastal Gulf of Alaska (Praetorius and Mix, 2014) show a period of intense iceberg calving around North Pacific beginning between  $\sim 18$  and 17 ka. Likewise, observations of surface freshening in the central Gulf of Alaska (Fig. 12c; Davies et al., 2011; Maier et al., 2018) suggest widespread calving of the western CIS beginning  $\sim 18$  ka.

Radiocarbon-dated marine sediments suggest that following the onset of deglaciation, marine-terminating CIS margins receded through fjords across Southeast Alaska and British Columbia until about  $\sim 15$  ka (Mann and Hamilton, 1995; Barrie and Conway, 1999; Lacourse and Mathewes, 2005). In the central Gulf of Alaska, sea surface salinity and ice-rafted debris deposition decreased between  $\sim 16$  and 15 ka (Fig. 12c; Maier et al., 2018), indicating that some formerly marine-terminating CIS termini began to recede onto land at this time, which reduced the delivery of icebergs and ice sheet meltwater to the open ocean. Radiocarbon-dated glaciomarine sediments from core EW0408-85JC on the southern Alaskan margin (Fig. 1) suggest major CIS outlet glaciers had transitioned from marine-terminating to land-terminating by  $\sim 14.8$  ka (Davies et al., 2011). This period coincides with an interval of marked CIS thinning in coastal British Columbia (Darvill et al., 2018), and evidence from Baker Island demonstrates that local glaciers in coastal Southeast Alaska also disappeared by  $\sim 15.5$  ka (Fig. 6; Lesnek et al., 2018). Taken together, the available data point to widespread retreat of marine-terminating CIS margins between  $\sim 18$  and 15 ka.

Retreat of western CIS margins continued after  $\sim 15$  ka, and by the early Holocene what remained of the CIS was restricted to mainland British Columbia (Margold et al., 2013; Margold et al., 2014; Menounos et al., 2017). In the absence of major CIS outlet glaciers, high-elevation areas fringing the Pacific coast likely hosted small, localized ice caps and cirque glaciers (Fedje and Mathewes, 2005), but the history of glacier change along the Pacific coast between

$\sim 15$  ka and the onset of the Holocene at 11.7 ka is unknown. Glacier readvances in the interior regions of British Columbia occurred during the Younger Dryas (Menounos et al., 2017), but from the data presented here, it is unclear if similar readvances occurred in Southeast Alaska. Additional detailed, site-specific work should take place to further constrain Younger Dryas and Holocene glacier fluctuations in Southeast Alaska. By 11 ka, ice in western Canada had retreated significantly from its late Pleistocene maximum (Clague, 2017), consistent with our results from the Southeast Alaskan coast.

## Causes of marine-terminating Cordilleran Ice Sheet change

The shift from the end of the LGM ( $\sim 19$  ka) to the start of the Holocene interglacial was accompanied by dramatic changes in global eustatic sea level (Spratt and Lisiecki, 2016), ocean temperature (Bereiter et al., 2018), and air temperature (Shakun et al., 2012). In addition, the glaciological structure of the CIS may have shifted when the ice sheet reached its maximum volume, resulting in the formation of large ice streams in many regions along the Pacific coast (Eyles et al., 2018). In this section, we explore the potential impact of each of these factors on CIS change in Southeast Alaska and western British Columbia during the last deglaciation.

Based on our record in coastal Southeast Alaska as well as other records across the North Pacific (Blaise et al., 1990; Cosma and Hendy, 2008; Praetorius and Mix, 2014; Praetorius et al., 2016; Maier et al., 2018), the period between  $\sim 18$  and 15 ka was one of intense calving of marine-terminating CIS margins. One mechanism that may have triggered widespread ice sheet retreat was sea level rise in the early deglacial period. Somewhat unusually for recently deglaciated landscapes (which typically experience relative sea level fall due to isostatic rebound), sea level in Southeast Alaska and western British Columbia likely rose during the early deglacial period due to a combination of eustatic sea level rise (Fig. 12b; Spratt and Lisiecki, 2016) and the migration and collapse of a crustal forebulge (Addison et al., 2010; Shugar et al., 2014; Carlson and Baichtal, 2015). These two processes, when working together, could have destabilized grounded ice margins and driven iceberg production (Clague, 1989) during the early deglacial period. The presence of streamlined bedforms in troughs around the Pacific coast suggests that CIS outlet glaciers (and possibly ice streams; see Eyles et al., 2018) in Southeast Alaska and British Columbia were grounded in their fjords when the CIS was at its maximum extent (Herzer and Bornhold, 1982; Blaise et al., 1990). These fast-flowing ice margins may have been especially vulnerable to sea-level-driven instability (Hendy and Cosma, 2008; Bassis et al., 2017; Eyles et al., 2018).

Warming of the ocean in contact with ice sheet margins may have contributed to initial CIS retreat at  $\sim 17$  ka (Joughin et al., 2012), and several studies have documented major changes in eastern Pacific Ocean conditions during the last deglaciation. On the Vancouver Island shelf, Mg/Ca ratios

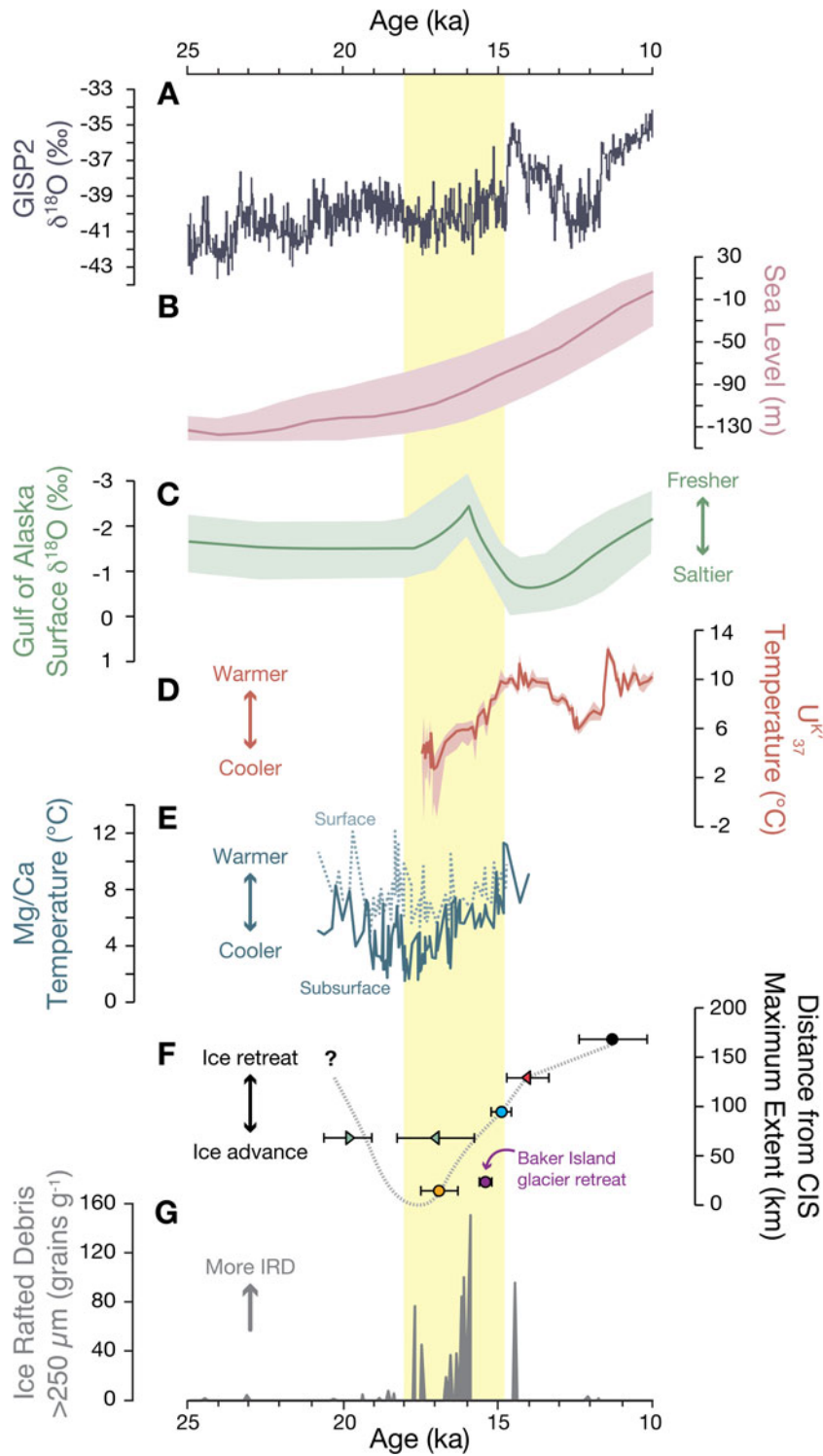


**Figure 12.** Glacial and climate history of the Pacific coast. (A) GISP2  $\delta^{18}\text{O}$  (Grootes and Stuiver, 1997). (B) Global eustatic sea level stack (Spratt and Lisiecki, 2016). (C) Gulf of Alaska surface  $\delta^{18}\text{O}$  from marine sediment core SO202-27-6, which relates to salinity (Maier et al., 2018). (D) Sea surface temperatures derived from alkenones in marine sediment core EW0408-85JC (Praetorius et al., 2015). (E) Surface (light blue dotted line) and subsurface (dark blue solid line) ocean temperatures derived from Mg/Ca ratios in foraminifera in marine sediment core MD02-2946 (Taylor et al., 2014). (F) Time distance diagrams for the marine-terminating CIS margin in coastal Southeast Alaska. Circles represent average  $^{10}\text{Be}$  ages plotted against distance from the CIS maximum extent, color coded by group. Triangles are  $^{14}\text{C}$  ages; green triangles are  $^{14}\text{C}$  ages on ringed seal bones in Shuká Káa (Lesnek et al., 2018), pink triangles are on shells in raised marine sediments (this study). (G) Ice-rafted debris in marine sediment core MD02-2946, offshore Vancouver Island (Cosma and Hendy, 2008). (For interpretation of the references to color in this figure legend, the reader is referred to the web version of this article.)



in surface- and subsurface-dwelling foraminifera show warming of  $\sim 2^{\circ}\text{C}$  and  $\sim 5^{\circ}\text{C}$ , respectively, between  $\sim 17.2$  and  $15$  ka (Fig. 12e; Taylor et al., 2014). A similar warming trend was underway by  $\sim 18$  ka on the Gulf of Alaska shelf, with peak temperatures reached by  $\sim 14$  ka following a warming of  $\sim 9^{\circ}\text{C}$ . (Fig. 12d; Praetorius et al., 2015). However, between  $\sim 14$  and  $12$  ka (i.e., during the Bølling-Allerød and Younger Dryas), surface temperatures in the Gulf of Alaska decreased by  $\sim 5^{\circ}\text{C}$  (Praetorius et al., 2015). Due to the lack of detailed glacial chronology in Southeast Alaska during this interval, the influence of these fluctuations in ocean temperature just before the Pleistocene-Holocene transition on CIS and local glacier mass balance is unknown.

Changes in atmospheric temperature and precipitation could have enhanced the CIS margin response to sea level rise and ocean warming. Yet, because the CIS covered much of the Pacific coast until  $\sim 15$  ka, terrestrial paleoclimate archives that span the early deglacial period are scarce. One of the few available continuous deglacial climate records comes from the Mt. Logan ice core; however, Fisher et al. (2008) suggest variations in ice core  $\delta^{18}\text{O}$  correlate to changes in source region rather than temperature, and the chronology in the earlier part of the record is somewhat imprecise. In Southeast Alaska, Ager (2019) generated a  $\sim 15$  ka pollen record from Hummingbird Lake on southwestern Baranof Island (Fig. 2). The pollen record from this site documents several shifts in vegetation communities (and thus climate) during the Pleistocene-Holocene transition. From  $\sim 15$  to  $14$  ka, pine (*Pinus*) species are the most abundant, which are interpreted to represent relatively warm temperatures. Similarly, on Haida Gwaii, which is thought to have hosted only local glaciers during the LGM (Clague, 1989), terrestrial vegetation became established by  $\sim 15$  ka (Lacourse and Mathewes, 2005), suggesting the first significant post-glacial warming did not occur until then (Mathewes and Clague, 2017). In Hummingbird Lake, increases in alder (*Alnus*) pollen percentage and decreases in pine pollen percentage between  $\sim 14$  and  $11$  ka suggest that air temperatures generally cooled, a result that is consistent with marine temperature reconstructions across the North Pacific (Taylor et al., 2014; Praetorius et al., 2015). If this cooling occurred during the summer months, it may have slowed CIS retreat, or perhaps even triggered readvances of the CIS and/or local glaciers before the onset of the Holocene (e.g., Menounos et al., 2017).

Our results indicate that local glaciers (in the eastern region) and persistent snow patches (in the western and central regions) lingered in coastal Southeast Alaska until the early Holocene. What caused the demise of these glaciers and snow patches? At present, terrestrial climate conditions in the region have been reconstructed from pollen assemblages and speleothem records. The appearance of Sitka spruce (*Picea sitchensis*), mountain hemlock (*Tsuga mertensiana*), and western hemlock (*Tsuga heterophylla*) pollen in Hummingbird Lake sediments after  $\sim 11$  ka is interpreted as a response to warming summer air temperatures at the beginning of the Holocene (Ager, 2019). These interpretations from pollen are corroborated by cave deposits from El

Capitan Cave on northern Prince of Wales Island (Fig. 2; Wilcox et al., 2019). There, a hiatus in speleothem deposition between  $41.5 \pm 0.2$  and  $13.4 \pm 0.2$  ka BP suggests the presence of discontinuous permafrost and/or the CIS, and therefore mean annual air temperatures below  $0^{\circ}\text{C}$ , during MIS 2 and the early deglacial period. Stable oxygen isotope measurements on speleothem material that dates from  $13.4 \pm 0.2$  to  $11.1 \pm 0.3$  ka BP show warming temperatures in the late Bølling-Allerød followed by mild cooling during the Younger Dryas, then a return to warmer conditions at the start of the Holocene (Wilcox et al., 2019). This interval of summertime warming in Southeast Alaska after  $\sim 11$  ka, identified in two independent archives, may have been sufficient to drive retreat of local glaciers in the Coast Mountains and also melt persistent snow patches in the western and central regions of the study area, resulting in surfaces with early Holocene exposure ages in these three regions (Figs. 6 and 10).

To summarize, in Southeast Alaska and western British Columbia, the initial retreat of marine-terminating CIS margins from their maximum extent was probably driven by factors acting on the ice-ocean interface, including sea level rise and ocean warming, leading to intense ice loss via calving in the early stages of deglaciation. The sensitive response of marine-terminating CIS regions to sea level and ocean temperature change during the early deglacial period may have been a consequence of the onset of ice streaming once the CIS reached its maximum volume (Eyles et al., 2018). During the later stages of deglaciation (after  $\sim 15$  ka), terrestrial climate reconstructions suggest that atmospheric warming also contributed to CIS margin recession.

## CONCLUSIONS

We present a new chronology for the recession of a marine-terminating CIS margin in southern Southeast Alaska. Our results suggest that ice retreat occurred in two pulses, with an initial phase occurring between  $\sim 17$  and  $15$  ka, as ice retreated from the outermost coast through the major fjords. This retreat may have been a result of eustatic sea level rise and oceanic warming acting in concert to destabilize grounded outlet glaciers and/or ice streams. After  $\sim 15$  ka, the CIS retreated into inland British Columbia, eventually leaving only small, localized ice caps in high-elevation areas that receded by  $\sim 11$  ka. Due to a lack of chronology between  $\sim 15$  and  $11$  ka, at this time our record cannot be used to assess the response of local glaciers in Southeast Alaska to hemispheric climate events such as the Younger Dryas. Overall, our reconstruction of deglaciation is consistent with other findings in marine-terminating CIS regions, suggesting a widespread response of the western CIS to deglacial climate change, including oceanic and perhaps atmospheric warming.

## ACKNOWLEDGMENTS

The authors would like to thank Risa J. Carlson, Jane L. Smith, Dennis J. Landwehr, Katherine Prussian, Anna Harris, and Nicholas

Schmuck for assistance in the field, and Christopher Sbarra for assistance in the field and the lab. Christopher Darvill and Nick Eyles provided thoughtful comments that improved this manuscript. Funding for this research was provided by an NSF Doctoral Dissertation Research Improvement Grant to Jason P. Briner and Alia J. Lesnek (award no. BCS-1657065) and by the Tongass National Forest Geology Program of the U.S. Forest Service.

## SUPPLEMENTARY MATERIAL

The supplementary materials for this article can be found at <https://doi.org/10.1017/qua.2020.32>.

## REFERENCES

- Addison, J.A., Beget, J.E., Ager, T.A., Finney, B.P., 2010. Marine tephrChronology of the Mt. Edgecumbe Volcanic Field, Southeast Alaska, USA. *Quaternary Research* 73, 277–292.
- Ager, T.A., 2019. Late Quaternary vegetation development following deglaciation of northwestern Alexander Archipelago, Alaska. *Frontiers in Earth Science* 7, 104.
- Ager, T.A., Carrara, P.E., Smith, J.L., Anne, V., Johnson, J., 2010. Postglacial vegetation history of Mitkof Island, Alexander Archipelago, southeastern Alaska. *Quaternary Research* 73, 259–268.
- Baichtal, J.F., Carlson, R.J., 2010. Development of a model to predict the location of early Holocene habitation sites along the western coast of Prince of Wales Island and the outer islands, Southeast Alaska. *Curr. Res. Pleistocene* 27, e67.
- Balco, G., 2017. Production rate calculations for cosmic-ray-muon-produced  $^{10}\text{Be}$  and  $^{26}\text{Al}$  benchmarked against geological calibration data. *Quaternary Geochronology* 39, 150–173.
- Balco, G., Stone, J.O., Lifton, N.A., Dunai, T.J., 2008. A complete and easily accessible means of calculating surface exposure ages or erosion rates from  $^{10}\text{Be}$  and  $^{26}\text{Al}$  measurements. *Quaternary Geochronology* 3, 174–195.
- Bamber, J.L., Westaway, R.M., Marzeion, B., Wouters, B., 2018. The land ice contribution to sea level during the satellite era. *Environmental Research Letters* 13, 063008.
- Barrie, J.V., Conway, K.W., 1999. Late Quaternary glaciation and postglacial stratigraphy of the northern Pacific margin of Canada. *Quaternary Research* 51, 113–123.
- Bassil, J.N., Petersen, S.V., Mac Cathles, L., 2017. Heinrich events triggered by ocean forcing and modulated by isostatic adjustment. *Nature* 542, 332–334.
- Bereiter, B., Shackleton, S., Baggenstos, D., Kawamura, K., Severinghaus, J., 2018. Mean global ocean temperatures during the last glacial transition. *Nature* 553, 39–44.
- Bierman, P.R., Marsella, K.A., Patterson, C., Davis, P.T., Caffee, M., 1999. Mid-Pleistocene cosmogenic minimum-age limits for pre-Wisconsinan glacial surfaces in southwestern Minnesota and southern Baffin Island: a multiple nuclide approach. *Geomorphology* 27, 25–39.
- Blaise, B., Clague, J.J., Mathewes, R.W., 1990. Time of maximum Late Wisconsin glaciation, West Coast of Canada. *Quaternary Research* 34, 282–295.
- Bronk Ramsey, C., 2009. Bayesian analysis of radiocarbon dates. *Radiocarbon* 51, 337–360.
- Carlson, R., 2007. *Current models for the human colonization of the Americas: the evidence from Southeast Alaska*. PhD dissertation, Cambridge University, England.
- Carlson, R.J., Baichtal, J.F., 2015. A predictive model for locating early Holocene archaeological sites based on raised shell-bearing strata in Southeast Alaska, USA. *Geoarchaeology* 30, 120–138.
- Carr, J.R., Stokes, C.R., Vieli, A., 2013. Recent progress in understanding marine-terminating Arctic outlet glacier response to climatic and oceanic forcing: twenty years of rapid change. *Progress in Physical Geography* 37, 436–467.
- Carrara, P.E., Ager, T.A., Baichtal, J.F., 2007. Possible refugia in the Alexander Archipelago of southeastern Alaska during the late Wisconsin glaciation. *Canadian Journal of Earth Sciences* 44, 229–244.
- Clague, J.J., 2017. Deglaciation of the Cordillera of Western Canada at the end of the Pleistocene. *Cuadernos de Investigación Geográfica* 43, 449–466.
- Clague, J.J., 1989. Cordilleran Ice Sheet. In: Fulton, R.J. (Ed.), *Quaternary Geology of Canada and Greenland*. Geological Society of America, Ottawa, pp. 40–42.
- Clague, J.J., Mathewes, R.W., Warner, B.G., 1982. Late Quaternary geology of eastern Graham Island, Queen Charlotte Islands, British Columbia. *Canadian Journal of Earth Sciences* 19, 1786–1795.
- Clark, P.U., Dyke, A.S., Shakun, J.D., Carlson, A.E., Clark, J., Wohlfarth, B., Mitrovica, J.X., Hostetler, S.W., McCabe, A.M., 2009. The Last Glacial Maximum. *Science* 325, 710–714.
- Clark, P.U., Shakun, J.D., Baker, P.A., Bartlein, P.J., Brewer, S., Brook, E., Carlson, A.E., Cheng, H., Kaufman, D.S., Liu, Z., 2012. Global climate evolution during the last deglaciation. *Proceedings of the National Academy of Sciences* 109, E1134–E1142.
- Corbett, L.B., Bierman, P.R., Graly, J.A., Neumann, T.A., Rood, D.H., 2013. Constraining landscape history and glacial erosivity using paired cosmogenic nuclides in Upernavik, northwest Greenland. *Geological Society of America Bulletin* 125, 1539–1553.
- Corbett, L.B., Bierman, P.R., Rood, D.H., 2016. An approach for optimizing in situ cosmogenic  $^{10}\text{Be}$  sample preparation. *Quaternary Geochronology* 33, 24–34.
- Cosma, T., Hendy, I.L., 2008. Pleistocene glacial marine sedimentation on the continental slope off Vancouver Island, British Columbia. *Marine Geology* 255, 45–54.
- Cosma, T.N., Hendy, I.L., Chang, A.S., 2008. Chronological constraints on Cordilleran Ice Sheet glaciomarine sedimentation from core MD02-2496 off Vancouver Island (western Canada). *Quaternary Science Reviews* 27, 941–955.
- Darvill, C., Menounos, B., Goehring, B., Lian, O., Caffee, M., 2018. Retreat of the western Cordilleran Ice Sheet margin during the last deglaciation. *Geophysical Research Letters* 45, 9710–9720.
- Davies, M., Mix, A., Stoner, J., Addison, J., Jaeger, J., Finney, B., Wiest, J., 2011. The deglacial transition on the southeastern Alaska Margin: meltwater input, sea level rise, marine productivity, and sedimentary anoxia. *Paleoceanography* 26, PA2223.
- Dyke, A.S., 2004. An outline of North American deglaciation with emphasis on central and northern Canada. In: Ehlers, J., Gibbard, P.L. (Eds.), *Developments in Quaternary Sciences*. Elsevier, pp. 373–424.
- Eyles, N., Moreno, L.A., Sookhan, S., 2018. Ice streams of the Late Wisconsin Cordilleran Ice Sheet in western North America. *Quaternary Science Reviews* 179, 87–122.
- Fedje, D.W., Mathewes, R.W., (Ed.s) 2005. *Haida Gwaii: Human History and Environment from the Time of Loon to the Time of the Iron People*. University of British Columbia Press, Vancouver.

- Fisher, D., Osterberg, E., Dyke, A., Dahl-Jensen, D., Demuth, M., Zdanowicz, C., Bourgeois, J., Koerner, R.M., Mayewski, P., Wake, C., 2008. The Mt Logan Holocene—late Wisconsinan isotope record: tropical Pacific—Yukon connections. *The Holocene* 18, 667–677.
- Groottes, P.M., Stuiver, M., 1997. Oxygen 18/16 variability in Greenland snow and ice with 10(–3)- to 10(5)-year time resolution. *Journal of Geophysical Research* 102, 26455–26470.
- Heaton, T.H., Grady, F., 2003. The late Wisconsin vertebrate history of Prince of Wales Island, Southeast Alaska. In: Schubert, B.W., Mead, J.L., Graham, R.W. (Eds.), *Ice Age Cave Faunas of North America*. Indiana University Press, Bloomington, IN, pp.17–53.
- Hendy, I., Cosma, T., 2008. Vulnerability of the Cordilleran Ice Sheet to iceberg calving during late Quaternary rapid climate change events. *Paleoceanography* 23, PA2101.
- Herzer, R.H., Bornhold, B.D., 1982. Glaciation and post-glacial history of the continental shelf off southwestern Vancouver Island, British Columbia. *Marine Geology* 48, 285–319.
- Hetherington, R., Barrie, J.V., Reid, R.G.B., MacLeod, R., Smith, D.J., James, T.S., Kung, R., 2003. Late Pleistocene coastal paleogeography of the Queen Charlotte Islands, British Columbia, Canada, and its implications for terrestrial biogeography and early postglacial human occupation. *Canadian Journal of Earth Sciences* 40, 1755–1766.
- Ives, P.C., Levin, B., Oman, C.L., Rubin, M., 1967. US Geological Survey radiocarbon dates IX. *Radiocarbon* 9, 505–529.
- Jones, R., Whitehouse, P., Bentley, M., Small, D., Dalton, A., 2019. Impact of glacial isostatic adjustment on cosmogenic surface-exposure dating. *Quaternary Science Reviews* 212, 206–212.
- Josephans, H., Fedje, D., Pienitz, R., Southon, J., 1997. Early humans and rapidly changing Holocene sea levels in the Queen Charlotte Islands-Hecate Strait, British Columbia, Canada. *Science* 277, 71–74.
- Joughin, I., Alley, R.B., Holland, D.M., 2012. Ice-sheet response to oceanic forcing. *Science* 338, 1172–1176.
- Kohl, C.P., Nishiizumi, K., 1992. Chemical isolation of quartz for measurement of in-situ -produced cosmogenic nuclides. *Geochimica et Cosmochimica Acta* 56, 3583–3587.
- Lacourse, T., Mathewes, R., 2005. Terrestrial paleoecology of Haida Gwaii and the continental shelf: vegetation, climate, and plant resources of the coastal migration route. In: Fedje, D.W., Mathewes, R.W. (Eds.), *Haida Gwaii: Human History and Environment from the Time of Loon to the Time of the Iron People*, University of British Columbia Press, pp. 38–58.
- Lal, D., 1991. Cosmic ray labeling of erosion surfaces: in situ nuclide production rates and erosion models. *Earth and Planetary Science Letters* 104, 424–439.
- Lesnek, A.J., Briner, J.P., Lindqvist, C., Baichtal, J.F., Heaton, T.H., 2018. Deglaciation of the Pacific coastal corridor directly preceded the human colonization of the Americas. *Science Advances* 4, eaar5040.
- Maier, E., Zhang, X., Abelmann, A., Gersonde, R., Mulitza, S., Werner, M., Méheust, M., Ren, J., Chapligin, B., Meyer, H., 2018. North Pacific freshwater events linked to changes in glacial ocean circulation. *Nature* 559, 241.
- Mann, D.H., 1986. Wisconsin and Holocene glaciation of southeast Alaska. In: Hamilton, T.D., Reed, K.M., Thomson, R.M. (Eds.), *Glaciation in Alaska: The Geologic Record*. Alaska Geographical Society, Anchorage, pp. 237–261.
- Mann, D.H., Hamilton, T.D., 1995. Late Pleistocene and Holocene paleoenvironments of the North Pacific coast. *Quaternary Science Reviews* 14, 449–471.
- Mann, D.H., Peteet, D.M., 1994. Extent and Timing of the Last Glacial Maximum in Southwestern Alaska. *Quaternary Research* 42, 136–148.
- Margold, M., Jansson, K.N., Kleman, J., Stroeven, A.P., Clague, J.J., 2013. Retreat pattern of the Cordilleran Ice Sheet in central British Columbia at the end of the last glaciation reconstructed from glacial meltwater landforms. *Boreas* 42, 830–847.
- Margold, M., Stroeven, A.P., Clague, J.J., Heyman, J., 2014. Timing of terminal Pleistocene deglaciation at high elevations in southern and central British Columbia constrained by Be–10 exposure dating. *Quaternary Science Reviews* 99, 193–202.
- Mathewes, R.W., Clague, J.J., 2017. Paleoecology and ice limits of the early Fraser glaciation (Marine Isotope Stage 2) on Haida Gwaii, British Columbia, Canada. *Quaternary Research* 88, 277–292.
- Menounos, B., Goehring, B.M., Osborn, G., Margold, M., Ward, B., Bond, J., Clarke, G.K., Clague, J.J., Lakeman, T., Koch, J., 2017. Cordilleran Ice Sheet mass loss preceded climate reversals near the Pleistocene termination. *Science* 358, 781–784.
- Misarti, N., Finney, B.P., Jordan, J.W., Maschner, H.D.G., Addison, J.A., Shapley, M.D., Krumhardt, A., Beget, J.E., 2012. Early retreat of the Alaska Peninsula Glacier Complex and the implications for coastal migrations of First Americans. *Quaternary Science Reviews* 48, 1–6.
- Nishiizumi, K., Imamura, M., Caffee, M.W., Southon, J.R., Finkel, R.C., McAninch, J., 2007. Absolute calibration of <sup>10</sup>Be AMS standards. *Nuclear Instruments and Methods in Physics Research Section B: Beam Interactions with Materials and Atoms* 258, 403–413.
- NSIDC, G.a., 2005, updated 2018. Global Land Ice Measurements from Space glacier database., in: Center, T.i.G.c.a.t.N.S.a.I.D. (Ed.), Boulder, CO.
- Praetorius, S., Mix, A., Jensen, B., Froese, D., Milne, G., Wolhowe, M., Addison, J., Prah, F., 2016. Interaction between climate, volcanism, and isostatic rebound in Southeast Alaska during the last deglaciation. *Earth and Planetary Science Letters* 452, 79–89.
- Praetorius, S., Mix, A., Walczak, M., Wolhowe, M., Addison, J., Prah, F., 2015. North Pacific deglacial hypoxic events linked to abrupt ocean warming. *Nature* 527, 362–366.
- Praetorius, S.K., Mix, A.C., 2014. Synchronization of North Pacific and Greenland climates preceded abrupt deglacial warming. *Science* 345, 444–448.
- Reimer, P.J., Bard, E., Bayliss, A., Beck, J.W., Blackwell, P.G., Ramsey, C.B., Buck, C.E., Cheng, H., Edwards, R.L., Friedrich, M., 2013. IntCal13 and Marine13 radiocarbon age calibration curves 0–50,000 years cal BP. *Radiocarbon* 55, 1869–1887.
- Shakun, J.D., Clark, P.U., He, F., Marcott, S.A., Mix, A.C., Liu, Z., Otto-Bliesner, B., Schmittner, A., Bard, E., 2012. Global warming preceded by increasing carbon dioxide concentrations during the last deglaciation. *Nature* 484, 49.
- Shugar, D.H., Walker, I.J., Lian, O.B., Eamer, J.B.R., Neudorf, C., McLaren, D., Fedje, D., 2014. Post-glacial sea-level change along the Pacific coast of North America. *Quaternary Science Reviews* 97, 170–192.
- Spratt, R.M., Lisiecki, L.E., 2016. A Late Pleistocene sea level stack. *Climate of the Past* 12, 1079–1092.
- Staiger, J., Gosse, J., Toracinta, R., Oglesby, B., Fastook, J., Johnson, J.V., 2007. Atmospheric scaling of cosmogenic nuclide



- production: climate effect. *Journal of Geophysical Research: Solid Earth* 112, B02205.
- Taylor, M.A., Hendy, I.L., Pak, D.K., 2014. Deglacial ocean warming and marine margin retreat of the Cordilleran Ice Sheet in the North Pacific Ocean. *Earth and Planetary Science Letters* 403, 89–98.
- Viens, R.J., 2001. *Late Holocene climate change and calving glacier fluctuations along the southwestern margin of the Stikine Icefield, Alaska*. PhD dissertation, University of Washington, Seattle.
- Walker, M., Johnsen, S., Rasmussen, S.O., Popp, T., Steffensen, J.P., Gibbard, P., Hoek, W., Lowe, J., Andrews, J., Björck, S., 2009. Formal definition and dating of the GSSP (Global Stratotype Section and Point) for the base of the Holocene using the Greenland NGRIP ice core, and selected auxiliary records. *Journal of Quaternary Science* 24, 3–17.
- Warner, B.G., Mathewes, R.W., Clague, J.J., 1982. Ice-free conditions on the Queen-Charlotte Islands, British Columbia, at the height of the Late Wisconsin Glaciation. *Science* 218, 675–677.
- Weingartner, T.J., Danielson, S.L., Royer, T.C., 2005. Freshwater variability and predictability in the Alaska Coastal Current. *Deep Sea Research Part II: Topical Studies in Oceanography* 52, 169–191.
- Wilcox, P.S., Dorale, J.A., Baichtal, J.F., Spötl, C., Fowell, S.J., Edwards, R.L., Kovarik, J.L., 2019. Millennial-scale glacial climate variability in Southeastern Alaska follows Dansgaard-Oeschger cyclicity. *Scientific Reports* 9, 7880.
- Wilson, F.H., Hults, C.P., Mull, C.G., Karl, S.M., 2015. Geologic map of Alaska. US Department of the Interior, US Geological Survey.
- Yehle, L.A., 1978. Reconnaissance engineering geology of the Petersburg area, southeastern Alaska, with emphasis on geologic hazards. US Geological Survey. Open-File Report 78–675.
- Young, N.E., Schaefer, J.M., Briner, J.P., Goehring, B.M., 2013. A <sup>10</sup>Be production-rate calibration for the Arctic. *Journal of Quaternary Science* 28, 515–526.